THE JOURNAL OF BIOLOGICAL CHEMISTRY VOL. 290, NO. 35, pp. 21264–21279, August 28, 2015

Adaptor Protein-1 Complex Affects the Endocytic Trafficking and Function of Peptidylglycine α-Amidating Monooxygenase, a Luminal Cuproenzyme*

Received for publication, January 26, 2015, and in revised form, July 2, 2015 Published, JBC Papers in Press, July 13, 2015, DOI 10.1074/jbc.M115.641027

Mathilde L. Bonnemaison[‡], Nils Bäck[§], Megan E. Duffy[¶], Martina Ralle[¶], Richard E. Mains[‖], and Betty A. Eipper[‡‖1]

From the Departments of [‡]Molecular Biology and Biophysics and [‖]Neuroscience, University of Connecticut Health Center, Farmington, Connecticut 06030, the [§]Department of Anatomy, Faculty of Medicine, University of Helsinki, FIN-00014 Helsinki, Finland, and the [¶]Department of Molecular and Medical Genetics, Oregon Health and Sciences University, Portland, Oregon 97239

Background: Trafficking of Atp7a, a copper pump, and PAM-1, a cuproenzyme, depends on adaptor protein-1 complex (AP-1).
Results: Disruption of AP-1-dependent late endosomal trafficking diminishes the ability of PAM to retain copper and produce amidated peptides.
Conclusion: Impaired AP-1 function alters luminal copper delivery to PAM.
Significance: Altered luminal cuproenzyme function may contribute to diseases associated with diminished AP-1 function.

The adaptor protein-1 complex (AP-1), which transports cargo between the *trans*-Golgi network and endosomes, plays a role in the trafficking of Atp7a, a copper-transporting P-type ATPase, and peptidylglycine α-amidating monooxygenase (PAM), a copper-dependent membrane enzyme. Lack of any of the four AP-1 subunits impairs function, and patients with MEDNIK syndrome, a rare genetic disorder caused by lack of expression of the σ1A subunit, exhibit clinical and biochemical signs of impaired copper homeostasis. To explore the role of AP-1 in copper homeostasis in neuroendocrine cells, we used corticotrope tumor cells in which AP-1 function was diminished by reducing expression of its μ1A subunit. Copper levels were unchanged when AP-1 function was impaired, but cellular levels of Atp7a declined slightly. The ability of PAM to function was assessed by monitoring 18-kDa fragment-NH_2 production from proopiomelanocortin. Reduced AP-1 function made 18-kDa fragment amidation more sensitive to inhibition by bathocuproine disulfonate, a cell-impermeant Cu(I) chelator. The endocytic trafficking of PAM was altered, and PAM-1 accumulated on the cell surface when AP-1 levels were reduced. Reduced AP-1 function increased the Atp7a presence in early/recycling endosomes but did not alter the ability of copper to stimulate its appearance on the plasma membrane. Co-immunoprecipitation of a small fraction of PAM and Atp7a supports the suggestion that copper can be transferred directly from Atp7a to PAM, a process that can occur only when both proteins are present in the same subcellular compartment. Altered luminal cuproenzyme function may contribute to deficits observed when the AP-1 function is compromised.

Copper is required for several essential biological processes, including mitochondrial respiration, skin pigmentation, iron transport, connective tissue and blood vessel formation, antioxidant defense, catecholamine synthesis, and peptide amidation (1). It is transported into cells via copper transporter 1, transferred to a cytosolic chaperone, and delivered to its final destinations. The cytosolic chaperone ATOX1 transfers copper to ATP7A and ATP7B, P-type ATPases that transport the metal from the cytosol into the lumen of the secretory pathway for incorporation into luminal cuproproteins. Luminal copper chaperones have not been identified (2), and it has been proposed that a His/Met-rich luminal loop in ATP7A plays an essential role in the delivery process (3, 4). To do so, ATP7A and its luminal cuproenzyme targets must co-localize in an appropriate organelle.

In neuroendocrine cells, ATP7A provides copper to peptidylglycine α-amidating monooxygenase (PAM),[2] an essential enzyme that requires copper to catalyze peptide amidation, one of the final steps in the production of bioactive peptides (5). The cytosolic adaptor protein-1 complex (AP-1) plays an essential role in the trafficking of both of these integral membrane enzymes (6, 7). In addition to driving the transport of proteins between the *trans*-Golgi network (TGN) and endosomes, AP-1 mediates secretory granule formation and maturation in neuroendocrine cells (7–9). The AP-1 complex is composed of four subunits as follows: two large subunits (γ and β1), a medium

* This work was supported, in whole or in part, by National Institutes of Health Grants DK-32949 (to B. A. E.), GM-090016 (to M. R.), and S10-RR-025512 (to M. R.). This work was also supported by grants from the Pérklen and Liv och Hälsa Foundations and Finska Läkaresällskapet (to N. B.). The authors declare that they have no conflicts of interest with the contents of this article.

[1] To whom correspondence should be addressed: Dept. of Molecular Biology and Biophysics, University of Connecticut Health Center, 263 Farmington Ave., Farmington, CT 06030. Tel.: 860-679-8898; Fax: 860-679-1885; E-mail: eipper@uchc.edu.

[2] The abbreviations used are: PAM, peptidylglycine α-amidating monooxygenase; TES, *N*-tris(hydroxymethyl)methyl-2-aminoethanesulfonic acid; POMC, proopiomelanocortin; TGN, *trans*-Golgi network; ICP-MS, inductively coupled plasma-mass spectrometry; JP, joining peptide; ITS, insulin/transferrin/selenium; BCS, bathocuproine disulfonate; ABI, ACTH biosynthetic intermediate; WGA, wheat germ agglutinin; APP, amyloid precursor protein; ANOVA, analysis of variance; Ab, antibody; PHM, peptidylglycine α-hydroxylating monooxygenase; CSFM, complete serum-free medium.

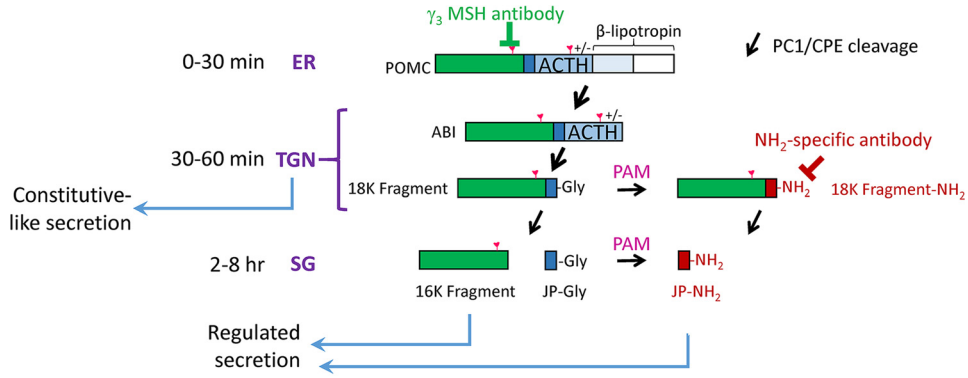

FIGURE 1. **POMC processing pathway and constitutive-like secretion.** The pathways leading from POMC to 18-kDa fragment-NH_2 and JP-NH_2 are illustrated. Cleavages by prohormone convertase 1/3 (PC1/3) proceed in the order indicated (30). The first cleavage generates ABI and β-lipotropin (data not shown). ABI is cleaved to produce 18-kDa fragment and ACTH (data not shown); 18-kDa fragment can be amidated by PAM only after carboxypeptidase E (*CPE*) removes the C-terminal basic amino acids, generating 18-kDa fragment Gly. Pulse-chase metabolic labeling studies demonstrated that about half of the 18-kDa fragment is amidated before further cleavage (21); cleavage by PC1/3 produces 16-kDa fragment and JP-NH_2 or JP-Gly, which is then amidated. Antibodies specific for the γ_3MSH region of POMC and for the amidated C terminus shared by 18-kDa fragment-NH_2 and JP-NH_2 were validated previously (21). *Red symbol*, *N*-linked glycan. These post-translational modifications occur as newly synthesized POMC travels through the secretory pathway. POMC cleavage begins in the TGN, and processing continues as immature secretory granules form mature secretory granules over a period of ~2 h. Secretion of the final products of POMC processing (16-kDa fragment, JP-NH_2, ACTH, and β-lipotropin) can be stimulated by application of secretagogues like $BaCl_2$. Secretion of several biosynthetic intermediates (ABI, 18-kDa fragment) occurs in the absence of a stimulus and is referred to as constitutive-like secretion.

subunit (μ1), and a small subunit (σ1); lack of any single AP-1 subunit impairs function (10–12).

Mutations in the AP1S1A gene, which encodes the σ1A subunit, cause MEDNIK (mental retardation, enteropathy, deafness, peripheral neuropathy, ichthyosis, and keratodermia) syndrome, an autosomal recessive disease characterized by altered copper homeostasis (1, 13). In sera from MEDNIK patients, ceruloplasmin, a copper-dependent secreted ferroxidase, and total copper levels are low, whereas free copper levels are elevated (1, 14). The major carrier of copper in serum, ceruloplasmin, incorporates copper during its biosynthesis; lacking copper, apoceruloplasmin is rapidly degraded in plasma (15). Despite normal intracellular copper levels, copper delivery to ceruloplasmin is impaired in MEDNIK patients (14). Analysis of fibroblasts from MEDNIK patients showed that ATP7A accumulates at the cell periphery instead of concentrating in the Golgi region (14). A similar shift in ATP7A localization was observed in HeLa cells with reduced levels of μ1A, a medium subunit, consistent with the need for all four subunits (6).

Using shRNA to decrease expression of the μ1A subunit to half, AP-1 was shown to play an essential role in secretory granule biogenesis and PAM trafficking in AtT-20 mouse corticotrope tumor cells (6, 7, 14). Although ATP7A trafficking in neuroendocrine cells has not been extensively explored, studies in other cell types predict an essential role for AP-1 (6, 14, 16, 17). AtT-20 cells produce proopiomelanocortin (POMC), a prohormone that is cleaved sequentially into a well characterized set of biosynthetic intermediates and product peptides that are either released constitutively or stored in secretory granules for release in response to secretagogue (Fig. 1). Production of the amidated products of POMC (18-kDa fragment-NH_2, JP-NH_2, and ACTH(1–13)NH_2) requires both PAM and Atp7a (5). We used well characterized assays for the amidation of POMC products to determine whether a modest reduction in AP-1 levels altered copper levels, Atp7a trafficking, or PAM function. Our data are most consistent with the hypothesis that Atp7a transfers copper directly to PAM at a site near the TGN.

Experimental Procedures

Antibodies—The antibodies used in this study are summarized in Table 1. The generation of the following antibodies was previously described: Atp7a (C terminus) (17); C-STOP (18); exon 16 (19); PHM (20); POMC (21); ACTH (22); JP-NH_2 (23); and TGN38 (24). The specificity of the Atp7a antibody for Western blotting and for immunostaining was established previously (25).

Cell Culture and Generation of Scramble and sh-μ1A PAM-1 Cells—AtT-20 cells were grown at 37 °C with 5% CO_2 in Dulbecco's modified Eagle's medium/F-12 (DMEM/F-12) containing 25 mM HEPES, 100 units/ml penicillin, 100 μg/ml streptomycin, 10% fetal bovine serum, 10% NuSerum. AtT-20 cells stably expressing PAM-1 were described previously (26). Generation of sh-μ1A and scramble PAM-1 AtT-20 cells using lentivirus targeted to μ1A (Sigma; clone ID TRCN0000111549) and a nontarget shRNA (Sigma, catalog no. SHC002V), respectively, was described previously (7).

Immunofluorescent Staining—Cells were plated onto 0.16–0.19-mm-thick glass, 12-mm round coverslips (Fisher) or 4-chamber glass slides. Both supports were coated with 0.1 mg/ml poly-L-lysine for 5 min followed by a rinse in NuSerum and two rinses in growth medium. Cells were fixed in 4% formaldehyde in PBS (50 mM NaH_2PO_4, 150 mM NaCl, pH 7.4) for 20 min at room temperature or in methanol at −20 °C. After rinsing in PBS, formaldehyde-fixed cells were permeabilized in 0.075% Triton X-100, 2 mg/ml BSA in PBS for 20 min at room temperature and then incubated in block (2 mg/ml BSA in PBS) for 20 min at room temperature. Primary antibodies diluted in block were incubated with the cells overnight at 4 °C. After three rinses in PBS, cells were incubated for 1 h at room temperature in block containing either fluorescein isothiocyanate-(FITC, 1:500 dilution) or Cy3 (1:2000 dilution)-conjugated donkey antibody to mouse or rabbit immunoglobulin (Jackson ImmunoResearch). After three rinses in PBS, cells were incubated with Hoechst 33342 (1:1000 dilution in PBS; Invitrogen)

TABLE 1
Antibody list

Antigen	Working dilution	Identity, source
Atp7a (CT77, C terminus)	1:1000	17
Atp7a (N terminus)	1:1000	NeuroMAb
APP (22C11)	1:1000	Millipore
Rat PAM		
C-STOP, PAM-1(965–976)	1:1000	18
Exon 16, PAM-1(409–497)	1:1000	19
Secretory granule proteins		
POMC (γ_3MSH)	1:1000	21
JP-NH_2	1:1000	23
ACTH (C terminus)	1:4000	21
ACTH (C terminus)	1:1000	Abcam (clone 56)
AP-1 components		
μ1A	1:500	ProteinTech Group
γ-Adaptin	1:1000	BD Biosciences
Golgi markers		
GM130	1:1000	BD Biosciences
TGN38(155–249)	1:1000	24
Syntaxin 6	1:50	BD Biosciences
EEA1	1:50	Santa Cruz Biotechnology

for 10 min at room temperature. After three rinses in PBS, cells were mounted using ProLong® Gold (Invitrogen).

Quantification of Images—Cells were visualized using a Nikon TE300 epifluorescence microscope with an oil immersion ×63 Plan Apochromat objective (NA 1.4). Quantification of fluorescence images was done using NIS Elements software. Background values were determined by measuring the average intensity in parts of the picture without cells for both green and red images. Background was then subtracted for both green and red images using the average intensity measured as a constant value for the entire image. Three regions were identified in each cell analyzed as follows: Golgi (based on staining for GM130) and nucleus and cytosol (region distinct from nucleus and Golgi). For each cell, two identically sized boxes were drawn; one box was placed over the Golgi, and the other box was placed over the cytosol. The average fluorescence signal intensity in each region was measured for 8–41 cells. Cytosol/Golgi fluorescence intensity ratios are shown. Statistical analyses were made using paired *t* tests on the ratios calculated.

For confocal analyses, cells were visualized using a Zeiss LSM 510-Meta with an oil immersion ×63 Plan Apochromat objective (NA 1.4). Co-localization of markers was assessed using Metamorph. For each image, colors were first separated, and the background was subtracted as described above. For each color, the image was thresholded using an inclusive threshold at least three times background. Co-localization of markers was measured based on area. Statistical analyses were made using paired *t*-tests on the ratios calculated.

For quantification of PAM endocytic trafficking to the TGN, cells were incubated with PAM exon 16 antibody (1:1000 in DMEM/HEPES, 0.2 mg/ml BSA) at 37 °C for 5 min, then chased in culture medium for 5 or 15 min and fixed in methanol. The fixed cells were incubated with antibody to syntaxin 6 followed by Alexa 488-conjugated goat anti-mouse and Alexa 555-conjugated goat anti-rabbit IgG (both 1:200) and visualized with a Leica TCS SP8 MP CARS microscope with a glycerol immersion ×63 objective (NA 1.3). For each group in each experiment, 15 areas covering about three cells were systematically sampled with single scans through the TGN area. Manders' coefficients, which indicate the proportion of the PAM immunoreactivity that overlaps syntaxin 6 staining, were determined using the JACoP plugin of ImageJ (27).

Electron Microscopy—To label early endocytic compartments, cells were incubated with 30 μg/ml wheat germ agglutinin linked to horseradish peroxidase (WGA-HRP) (Sigma) on ice for 30 min, then chased in culture medium for 10 min at 37 °C, and fixed with 1.5% glutaraldehyde in 0.1 M phosphate buffer. The fixed cells were then incubated with 0.25 mg/ml diaminobenzidine in 0.05 M Tris-HCl, pH 7.6, and 0.65 mg/ml hydrogen peroxide for 10 min on ice, post-fixed with 1% osmium tetroxide and 1.5% potassium ferrocyanide, dehydrated, and embedded in Epon. Sections were post-stained with uranyl acetate and lead citrate.

For colloidal gold labeling of endosomal structures, cells were incubated with a PAM ectodomain antibody (PAM exon 16; 1:250 in DMEM/HEPES, 1 mg/ml BSA) for 30 min at 4 °C, rinsed with DMEM/HEPES/BSA at 4 °C, incubated in DMEM/HEPES with protein A, 15 nm colloidal gold (University of Utrecht, Utrecht, Netherlands) at the concentration suggested by the provider (1:60–75) for 30 min at 4 °C, rinsed in DMEM/HEPES at 4 °C, and then chased in culture medium at 37 °C. After a 10- or 20-min chase, cells were fixed with 2.5% glutaraldehyde in 0.1 M sodium cacodylate buffer and osmicated, dehydrated, and embedded in Epon as described above. Sections were systematically scanned for gold particle-containing endosomal structures, yielding 20 labeled structures (~100 gold particles) for each group in each experiment.

Inductively Coupled Plasma-Mass Spectrometry (ICP-MS)—Tubes used for ICP-MS were incubated in 1% HNO_3 (trace metal grade, Fisher) for at least 24 h. Scramble and sh-μ1A PAM-1 cells were plated onto a 6-well dish. When confluent, cells were trypsinized and resuspended in HSG buffer (15 mM HEPES, 120 mM NaCl, 2 mM $CaCl_2$, 4 mM KCl, 25 mM glucose, pH 7.4). Resuspended cells were split into 3 equal aliquots, which were used for cell counting, measurement of protein concentration, and ICP-MS. Cells for ICP-MS were pelleted, and the supernatant was discarded. Samples were digested with 200 μl of 50% HNO_3 (trace metal grade, Fisher) in Eppendorf tubes at room temperature overnight. The digested samples were brought to a total volume of 1 ml with 1% HNO_3, mixed by vortexing, and spun at 3500 × *g* for 3 min to remove debris. ICP-MS analysis was carried out in the Elemental Analysis Core at Oregon Health and Science University using an Agilent 7700x equipped with an ASX 250 autosampler. The system was operated at a radio frequency power of 1550 watts, an argon plasma gas flow rate of 15 liter/min, and argon carrier gas flow rate of 1.08 liters/min. Elements were measured in kinetic energy discrimination mode using helium gas (4.2 ml/min). For measurement, samples were transferred to acid-treated 15-ml conical tubes. Data were quantified using a 9-point calibration standard (Common Elements Mix 2 Multi-Element Aqueous Standard, VHG Labs) in 1% HNO_3. For each sample, data were acquired in triplicate and averaged. A Ge-72 internal standard (Internal Standard Multi-Element Mix 3, VHG Labs) introduced with the sample was used to correct for plasma instabilities, and frequent measurements of a 10 ppb all-analyte solu-

tion as well as a blank (containing 1% HNO_3 only) were used as quality control and to determine the coefficient of variance. To assess recovery rates of elements and probe background contamination from containers, a certified NIST standard reference material (Trace Elements in Water, 1643e) was digested and analyzed by the same method as the samples. HSG buffer was also analyzed to determine background contributions.

Primary Anterior Pituitary Cell Culture—Rat anterior pituitary cells were plated on 0.16–0.19-mm-thick glass, 12-mm round coverslips (Fisher) coated with 0.1 mg/ml poly-L-lysine for 5 min followed by a rinse in NuSerum and two rinses in AtT-20 growth medium as described previously (28). Briefly, rat anterior pituitary was rinsed in CSFM/air medium (DMEM/F-12 air, 25 mM HEPES, 100 units/ml penicillin, 100 μg/ml streptomycin, 1–2 mg/ml BSA, ITS, 50 μM ascorbate) and diced. Pituitary pieces were incubated in 0.75 ml of collagenase solution (4 mg/ml crude collagenase, 1 mg/ml hyaluronidase, 0.1 unit/ml benzonase, 10 mg/ml BSA) for 20 min at 37 °C without CO_2 under agitation. Pituitary fragments were diluted with 14 ml of CSFM/air and spun down at room temperature for 5 min. Supernatant was removed, and cells were incubated with 0.75 ml of 3 mg/ml trypsin I-300 dissolved in CSFM/air for 5 min at 37 °C without CO_2 under agitation. Trypsin was blocked by adding 0.75 ml of 0.2 mg/ml lima bean trypsin inhibitor dissolved in AtT-20 medium. The dissociated cells were then filtered through a 70-μm filter. After centrifugation of the flow-through, the cell pellet was resuspended in 5 ml of 160 mM NH_4Cl to lyse red blood cells and then spun again for 5 min at room temperature. The cell pellet was resuspended in 5 ml of AtT-20 growth medium. 1/25th of a rat anterior pituitary was plated per well of a 24-well dish. Cells remained in AtT-20 growth medium for 2 days and were then switched to DMEM/F-12, 25 mM HEPES, 100 units/ml penicillin, 100 μg/ml streptomycin, 1–2 mg/ml BSA, ITS, 50 μM ascorbate. Cells were used on days 3 and 4.

Manipulation of Cells—Cells were incubated in DMEM/F-12 air medium containing 25 mM HEPES, pH 7.4, 1 mg/ml BSA for 30 min at 37 °C without CO_2. For transferrin uptake experiments, cells were then incubated in DMEM/F-12 air medium containing 25 mM HEPES, pH 7.4, 1 mg/ml BSA, 25 μg/ml Alexa Fluor 546 transferrin (Life Technologies, Inc.) for 10 min at 37 °C without CO_2. Cells were fixed using 4% formaldehyde in PBS for 20 min at room temperature. For nocodazole treatment experiments, cells were incubated for 10 min at 37 °C in DMEM/F-12 air medium containing 25 mM HEPES, pH 7.4, 1 mg/ml BSA, and 10 μM nocodazole (Sigma) or the equivalent volume of DMSO followed by 10 min in the same medium containing 25 μg/ml Alexa Fluor 546 transferrin.

BCS and Copper Treatment of AtT-20 Cells—Cells were first incubated for 30 min in DMEM/F-12 medium or DMEM/F-12 air medium containing ITS, 25 mM HEPES, pH 7.4, 1 mg/ml BSA. Cells were equilibrated in this medium during two consecutive 30 min incubations at 37 °C with 5% CO_2 (DMEM/F-12 medium) or without CO_2 (DMEM/F-12 air medium). Cells were then treated with medium containing 50 μM bathocuproinedisulfonic acid (BCS, Sigma) overnight or $CuCl_2$ (20 or 200 μM, Sigma) for 2 h or medium only as a control. Cells were either fixed for immunostaining, lysed in detergent for biochemical analysis, or chilled for cell surface biotinylation. Using an antibody against the C terminus of Atp7a (17), we observed a 2-fold increase in signal when AtT-20 cells were exposed to 20 μM copper for 2 h. The inability of cycloheximide, a protease synthesis inhibitor, to block this increase and the failure of an N-terminally directed Atp7a antibody to detect the increase suggested the occurrence of a copper-responsive post-translational modification.

Detection of JP Amidation—Antibody specific to the amidated C terminus of JP was generated by linking D-Tyr-Pro-Glu-Pro-Ser-Pro-Arg-Glu-NH_2 (D-Tyr-JP(12–18)NH_2) to BSA as described (23). The addition of a Gly residue to the C terminus of this peptide (JP(12–19)) reduced its cross-reactivity with this antiserum by 10,000-fold (23). For Western blot analysis, a fraction enriched in immunoglobulin by precipitation with ammonium sulfate (45% saturation) was dialyzed into 100 mM sodium phosphate, pH 7.4, and incubated with JP(12–19) linked to Affi-Gel15 beads (4 mg of peptide/2 ml of resin) for 1 h at 4 °C to remove any antibodies capable of recognizing this peptide. The unbound fraction was applied to a column of JP(12–18)NH_2 linked to Affi-Gel10 beads (5 mg of peptide/2 ml of resin); bound antibodies were eluted with 0.2 M glycine HCl, 0.1 M NaCl, 0.1% Triton X-100, pH 2.3; the eluate was rapidly neutralized with 3 M Tris-HCl, pH 8.0, and BSA (final concentration in eluate = 0.2 mg/ml) was added before dialysis against 100 mM sodium phosphate, pH 7.4. Preparation of an antibody specific for mouse POMC(76–100) (γ_3MSH) (21) was described previously. Affinity purification was carried out as described above using bovine γ_3MSH linked to Affi-Gel10 beads.

ELISA—Protein A-coated plates (Pierce) were rinsed three times with 200 μl of Tween/Tris-buffered saline (TTBS: 0.5% Tween 20, 50 mM Tris, 150 mM NaCl, pH 7.5). Affinity-purified JP-NH_2 antibody (1:1200 dilution), standard peptide (rat joining peptide; Phoenix Pharmaceuticals), and sample diluted into TTBS were allowed to bind to the strips for 2 h. Biotinylated JP-NH_2 (labeled using Pierce EZ-Link NHS-PEG4 biotinylation kit, per manufacturer's instructions; nominally 20 pg = 11 fmol per well) was added for 1 h. After four rinses (200 μl of TTBS), wells were incubated in 100 μl of 1:5000 Pierce high sensitivity streptavidin-HRP for 1 h, followed by TTBS rinses. Color was developed using 100 μl of 3,3′,5,5′-tetramethylbenzidine (Pierce 1-Step Ultra 3,3′,5,5′-tetramethylbenzidine-ELISA, diluted 1:3 in 100 mM sodium acetate, pH 5.0) for 5–10 min and stopped with 110 μl of 2 M H_2SO_4; OD was determined at 450 nm.

Biotinylation—AtT-20 cells plated in a 12-well plate were first incubated for 30 min in DMEM/F-12 air medium containing ITS, 25 mM HEPES, pH 7.4, 100 μg/ml BSA. Cells were equilibrated in air medium during two consecutive 30-min incubations at 37 °C without CO_2. Cells were then treated with air medium containing 20 μM $CuCl_2$ or air medium only as a control. Dishes were placed on ice and incubated for 10 min at 4 °C. Cells were rinsed with ice-cold HSG buffer (15 mM HEPES, 120 mM NaCl, 2 mM $CaCl_2$, 4 mM KCl, 25 mM glucose, pH 7.4). A solution containing 1.25 mM sulfo-NHS-LC-biotin (Thermo Scientific) in HSG buffer was made fresh and added to the cells for 10 min at 4 °C. After removing the biotin solution,

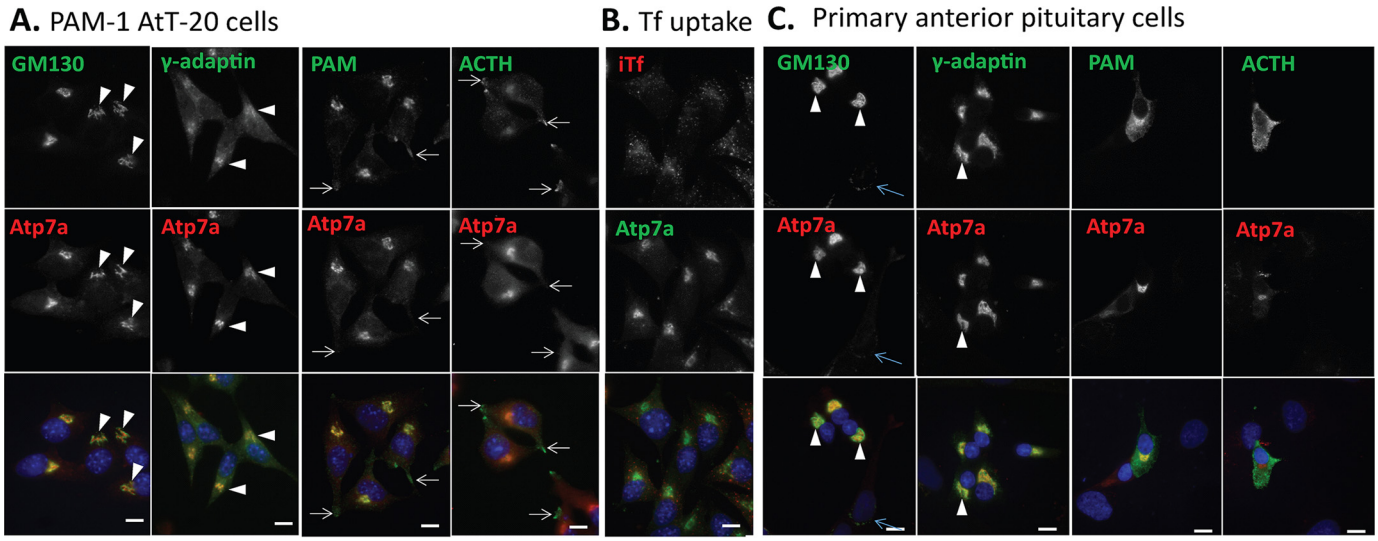

FIGURE 2. **Atp7a concentrates in the Golgi region in pituitary cells.** Indirect immunofluorescent staining of Atp7a (Cy3 anti-rabbit) and GM130 (a *cis*-Golgi marker; FITC anti-mouse), γ-adaptin (FITC anti-mouse), PAM (C terminus; FITC anti-mouse), or ACTH (secretory granule; FITC anti-mouse) in PAM-1 AtT-20 cells (*A*) and rat anterior pituitary cells (*C*) is shown. *White arrowheads* point to the Golgi; *white arrows* point to the tips, where secretory granules accumulate; *blue arrow* (*C*) points to a fibroblast. *B,* PAM-1 AtT-20 cells incubated with Alexa Fluor 546 transferrin for 10 min at 37 °C to identify early and recycling endosomes (*iTf*) were fixed and co-stained for Atp7a (FITC anti-rabbit). Nuclei were stained with Hoechst. *Scale bars,* 10 μm. Cells were visualized using a Nikon TE300 epifluorescence microscope.

cells were rinsed twice for 5 min with CSFM/air containing 2 mg/ml BSA. Cell extracts were collected using TMT (20 mM Na-TES, 10 mM mannitol, 1% Triton X-100, pH 7.4) containing a mixture of protease inhibitors (final concentrations 0.34 mg/ml phenylmethylsulfonyl fluoride, 50 μg/ml lima bean trypsin inhibitor, 2 μg/ml leupeptin, 16 μg/ml benzamidine, and 2 μg/ml pepstatin). Cells were solubilized in TMT for 30 min at 4 °C. Cell extracts were collected into microcentrifuge tubes and centrifuged at 22,000 × *g* for 15 min at 4 °C. Solubilized cell extracts were then incubated with streptavidin-agarose beads for 1 h at 4 °C. Beads were rinsed twice with TMT and once with TM (no Triton X-100). The bound fraction was eluted into Laemmli sample buffer by heating the samples for 5 min at 95 °C (PAM-1) or 55 °C (Atp7a).

Results

Atp7a, AP-1, and PAM Co-localize in the Golgi Region of AtT-20 Cells and Primary Pituitary Cells—We first compared the localization of endogenous Atp7a, γ-adaptin, and ACTH in AtT-20 cells stably expressing PAM-1 (PAM-1 AtT-20 cells). Unlike fibroblasts and HeLa cells, AtT-20 cells are professional secretory cells and store the products of prohormone processing in secretory granules for release in response to secretagogue. AtT-20 cells must deliver copper to the secretory pathway to support the synthesis of amidated peptides. Immunoelectron microscopy previously established the presence of PAM-1 in the tubulovesicular structures that constitute the TGN cisternae, immature secretory granules, and multivesicular bodies (24, 31, 32). Atp7a also concentrated in the perinuclear region, where its distribution overlapped that of the *cis*-Golgi marker, GM130, and γ-adaptin (Fig. 2*A*, *white arrowheads*).

Co-staining for Atp7a and PAM revealed extensive co-localization in the Golgi region. The generation of PAM substrates from POMC requires sequential endoproteolytic and exoproteolytic cleavages, which first occur in the TGN (Fig. 1) (21, 22). The tips of AtT-20 cells, where mature secretory granules containing 16-kDa fragment, JP-NH_2, ACTH, and the other final products of POMC processing accumulate, lack Atp7a (Fig. 2*A*, *white arrows* in *PAM* and *ACTH panels*). To identify early and recycling endosomes, Atp7a was visualized in cells that had been incubated with Alexa Fluor 546 transferrin before fixation (33); very little overlap between the internalized transferrin and Atp7a was observed (Fig. 2*B*, *iTf*).

To determine whether the Atp7a distribution in PAM-1 AtT-20 cells was representative of anterior pituitary endocrine cells *in vivo*, dissociated rat primary pituitary cells were maintained in culture for 4 days and then stained for Atp7a along with several organelle markers (Fig. 2*C*). As in PAM-1 AtT-20 cells, Atp7a localized to the Golgi region, where its distribution overlapped that of GM130 and γ-adaptin (Fig. 2*C*, *white arrowheads*). PAM expression varies in the different cell types found in the anterior pituitary (34). In cells expressing high levels of PAM, the amidating enzyme was largely localized in the Golgi region, where it co-localized with Atp7a (Fig. 2*C*). In corticotropes, ACTH-positive secretory granules were evenly distributed throughout the cell; although ACTH-positive secretory granules occupied most of the cellular space, Atp7a staining rarely overlapped staining for ACTH (Fig. 2*C*). In both AtT-20 cells and primary pituitary cells, any interaction between PAM and Atp7a would be expected to occur in the perinuclear region of the cell.

Decreased Expression of μ1A Alters Levels of Cuproproteins but Does Not Alter Intracellular Copper Levels—Because AP-1 is known to play a role in the formation of secretory granules and in the trafficking of Atp7a and PAM, we decided to use PAM-1 AtT-20 cells expressing different levels of AP-1 to explore copper delivery to this luminal cuproenzyme. AtT-20 cells stably expressing PAM-1 and infected with a lentivirus

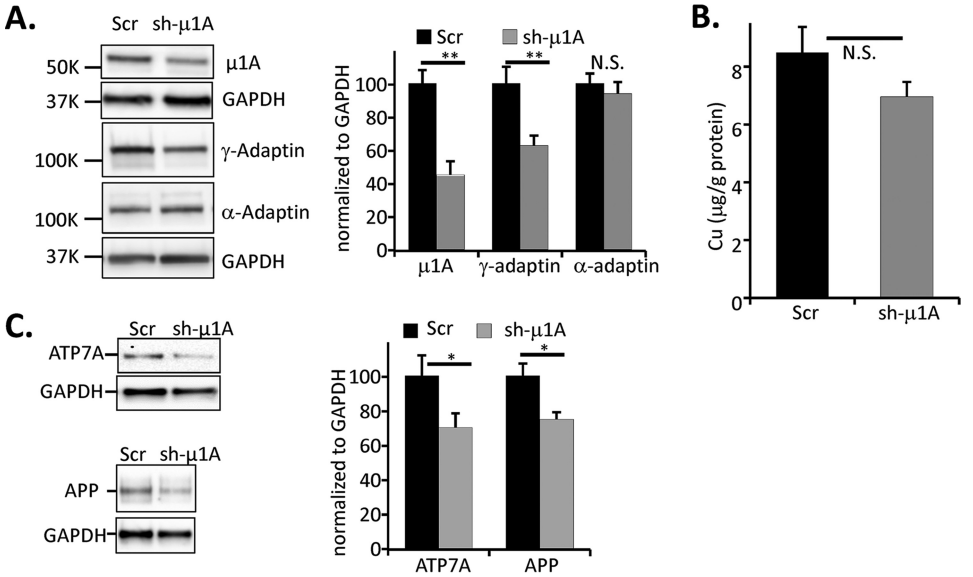

FIGURE 3. **Reduced μ1A levels in AtT-20 cells stably expressing PAM-1 alter Atp7a protein levels but do not alter copper levels.** *A,* levels of μ1A in sh-μ1A lysates were previously shown to be 50% of those in lysates of scramble (*Scr*) PAM-1 cells (7). Levels of another AP-1 subunit, γ-adaptin, and an AP-2 subunit, α-adaptin, were assessed to confirm the specificity of the knockdown; μ1A and γ-adaptin levels fell (**, $p < 0.01$), but α-adaptin levels were unaffected. Scr was normalized to 1.0. *B,* copper levels in scramble and sh-μ1A PAM-1 cells normalized to amount of protein (*N.S.,* not significant; $n = 6$; *error bars* represent S.E.). *C,* Western blots showing Atp7a and APP in scramble and sh-μ1A PAM-1 cells. *Graphs* indicate normalized levels of Atp7a and APP over GAPDH compared between scramble and sh-μ1A PAM-1 cells ($n = 5–8$; *, $p < 0.05$).

expressing an shRNA directed against μ1A (sh-μ1A) or a non-target shRNA (scramble) were described previously (7); levels of μ1A were reduced by a factor of about 2 (Fig. 3*A*). The TGN region of sh-μ1A PAM-1 cells is vacuolated; noncondensing secretory granules accumulate at the expense of immature secretory granules, and secretagogue-stimulated secretion is diminished (7). Although decreased expression of μ1A resulted in lower levels of another AP-1 subunit (γ-adaptin), we confirmed that levels of α-adaptin, an AP-2 subunit, were unaffected (Fig. 3*A*).

Intracellular copper levels in scramble and sh-μ1A PAM-1 cells were then compared using ICP-MS. No difference in intracellular copper levels was seen between scramble and sh-μ1A PAM-1 cells (Fig. 3*B*). Similarly, intracellular copper levels in skin fibroblasts from MEDNIK patients were within normal limits (42.5 ng/mg protein *versus* control range of 21.2 to 46.0 ng/mg protein) (14).

We turned to Western blot analysis to compare steady state levels of Atp7a and another protein whose luminal domain binds copper, amyloid precursor protein (APP) (35), in scramble and sh-μ1A PAM-1 cells. A 22 $\pm$ 9% decrease in the steady state levels of Atp7a in sh-μ1A PAM-1 cells was observed (Fig. 3*C*). APP trafficking in SH-SY5Y neuroblastoma cells is copper-dependent (36). APP levels were decreased by a similar amount (23 $\pm$ 4% decrease) in sh-μ1A PAM-1 cells (Fig. 3*C*). Although intracellular copper levels did not differ in sh-μ1A and scramble PAM-1 cells, levels of these two cuproproteins were reduced in sh-μ1A PAM-1 cells. To determine whether the ability of Atp7a to deliver copper to PAM was altered, we utilized an assay for 18-kDa fragment-NH_2, one of the amidated products produced from POMC (21).

Establishing an Assay for PAM Function in Intact Cells—To evaluate PAM function in scramble *versus* sh-μ1A PAM-1 AtT-20 cells, we took advantage of the fact that PC1/PC3-mediated cleavage of POMC produces two major amidated products (Fig. 1) (16, 17). Following cleavage at the C terminus of ACTH, cleavage at its N terminus reveals a potential amidation site (-Glu-Gly-Lys-Arg) at the C terminus of 18-kDa fragment; PAM cannot act until carboxypeptidase E or D has removed the C-terminal basic amino acids, revealing a C-terminal glycine, but these cleavages are followed quickly by amidation (21). An additional PC1/3-mediated cleavage can generate amidated joining peptide (JP-NH_2) and 16-kDa fragment (Fig. 1). Amidated POMC products are first detected in the TGN (22); pulse-chase studies indicate that amidation of both 18-kDa fragment and JP is completed within 1 h of synthesis (37). An antibody specific for 18-kDa fragment-NH_2 and JP-NH_2 was generated by immunizing rabbits with synthetic D-Tyr-Pro-Glu-Pro-Ser-Pro-Arg-Glu-NH_2; based on an ELISA, the affinity-purified NH_2-specific antibody cross-reacted less than 10,000 times as well with synthetic Pro-Glu-Pro-Ser-Pro-Arg-Glu-Gly (23). An affinity-purified γ_3MSH antibody (Fig. 1) was used to monitor levels of POMC, ABI, 18-kDa fragment, and 16-kDa fragment (21).

To identify the subcellular compartment in which PAM would be expected to convert 18-kDa fragment-Gly into 18-kDa fragment-NH_2, lysates and spent media prepared from Scr and sh-μ1A PAM-1 AtT-20 cells were examined (Fig. 4). As in our previous study (7), the γ_3MSH antibody detected similar amounts of differentially glycosylated POMC and 16-kDa fragment in lysates of Scr and sh-μ1A PAM-1 cells; consistent with previous metabolic labeling experiments, ABI and 18-kDa fragment were barely detectable in cell lysates (Fig. 4*A*). JP-NH_2, which has only 18 amino acids, does not bind to PVDF or nitrocellulose membranes and cannot be detected by Western blot. Analysis of the γ_3MSH-related products secreted during a 16-h collection period revealed a striking difference between Scr and sh-μ1A PAM-1 cells (Fig. 4*B*); although the total amount of

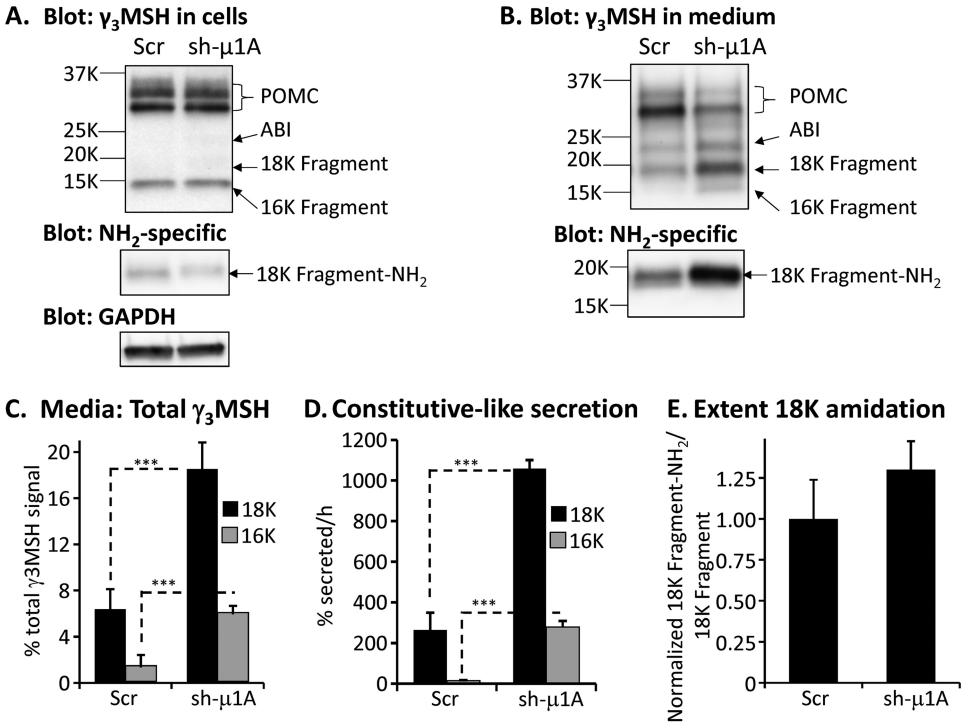

FIGURE 4. **Constitutive-like secretion of POMC products differs in scramble and sh-μ1A PAM-1 cells.** Cell lysates (*A*) and spent media (*B*) prepared from Scr and sh-μ1A PAM-1 cells incubated in CSFM for 16 h were fractionated and analyzed using the γ_3MSH-specific antibody, the NH_2-specific antibody, or an antibody to GAPDH; data were normalized to GAPDH. POMC products in the cell lysates were indistinguishable. *C,* although the total amount of γ_3MSH-related material secreted by scramble and sh-μ1A PAM-1 cells did not differ (γMSH total signal Scr = 1.00 $\pm$ 0.11 *versus* sh-μ1A = 0.87 $\pm$ 0.13, $n = 6$), the POMC products secreted by sh-μ1A PAM-1 cells were more extensively cleaved to 18-kDa fragment-NH_2 and 16-kDa fragment (two-way ANOVA; ***, $p < 0.001$). *D,* constitutive-like secretion of both 18-kDa fragment and 16-kDa fragment was elevated in sh-μ1A *versus* scramble PAM-1 cells (two-way ANOVA; ***, $p < 0.001$). *E,* secreted 18-kDa fragment was detected by the γ_3MSH-specific antibody and by the NH_2-specific antibody; the ratio of these signals provided a means of comparing the extent of amidation in scramble and sh-μ1A cells. No significant difference was observed.

cross-reactive material detected in the media did not differ, endoproteolytic cleavage was more extensive in sh-μ1A PAM-1 cells (Fig. 4*C*). Secretion of 18-kDa fragment-NH_2 by Scr PAM-1 cells was rapid, but its secretion by sh-μ1A PAM-1 cells was even faster (Fig. 4*D*). Despite these differences, comparison of the signals observed for 18-kDa fragment using the NH_2-specific antibody and the γ_3MSH-specific antibody revealed a similar extent of 18-kDa fragment amidation in Scr and sh-μ1A media (Fig. 4*E*). In both cell lines, the amidation of 18-kDa fragment by PAM must occur in the brief time following its cleavage from ABI and before its cleavage into 16-kDa fragment and JP-Gly. With normal levels of AP-1, this step occurs as 18-kDa fragment traverses immature secretory granules, a major site linking the biosynthetic and endocytic pathways (7).

PAM Function Is More Sensitive to Copper Chelation in sh-μ1A PAM-1 Cells—We reasoned that a significant alteration in copper homeostasis or protein trafficking caused by decreasing AP-1 function in PAM-1 AtT-20 cells might increase the sensitivity of PAM to limited copper availability. BCS, a cell impermeant Cu(I) chelator, is generally applied to cells at a level of 50–200 μM for 4–48 h (6, 38–40). In addition to depleting cellular copper levels by removing Cu(I) from the medium, BCS would be expected to remove copper from enzymes like PAM-1, which reach the plasma membrane after exocytosis, enter the endocytic pathway, and can be returned to secretory granules or degraded (31). Although the amount of PAM-1 on the cell surface at any given time is small, its flux onto and off of the cell surface is substantial. Based on our previous studies, it is estimated that all of the cellular PAM-1 could reside on the cell surface for 5 min in less than 2 h (31, 41). Bulk phase uptake of BCS could also provide access to copper in the lumen of the endocytic pathway.

We first asked how effective BCS and $CuCl_2$ were at altering copper levels in AtT-20 cells (Fig. 5*A*). AtT-20 cells were either treated with 50 μM BCS overnight, 20 μM $CuCl_2$ for 2 h, or remained untreated as a control. Copper levels were measured by ICP-MS. BCS treatment reduced copper levels by only about 30% (BCS: 4.11 $\pm$ 0.74 μg/g protein; no treatment: 5.63 $\pm$ 0.10 μg/g protein) and incubation with 20 μM $CuCl_2$ increased copper levels more than 6-fold ($CuCl_2$: 41.1 $\pm$ 3.9 μg/g protein).

We next asked whether the amidation of 18-kDa fragment in scramble and sh-μ1A PAM-1 cells exhibited differential sensitivity to BCS. Basal media and cell extracts from both cell lines were examined for POMC processing using the γ_3MSH-specifc antibody and for amidation using the 18-kDa fragment-NH_2-specific antibody (Fig. 5*B*). Neither the endoproteolytic cleavage of POMC nor secretion of its major cleaved products was altered by BCS treatment in scramble or sh-μ1A PAM-1 cells. In both scramble and sh-μ1A PAM-1 cells, BCS treatment produced a dose-dependent decrease in the amount of 18-kDa fragment-NH_2. Peptide amidation in scramble PAM-1 cells was decreased to about 50% of control when cells were treated with 20 μM BCS. In contrast, sh-μ1A PAM-1 cells were much more sensitive to BCS; peptide amidation decreased to about 50% of control when these cells were treated with 2 μM BCS (Fig. 5*B*).

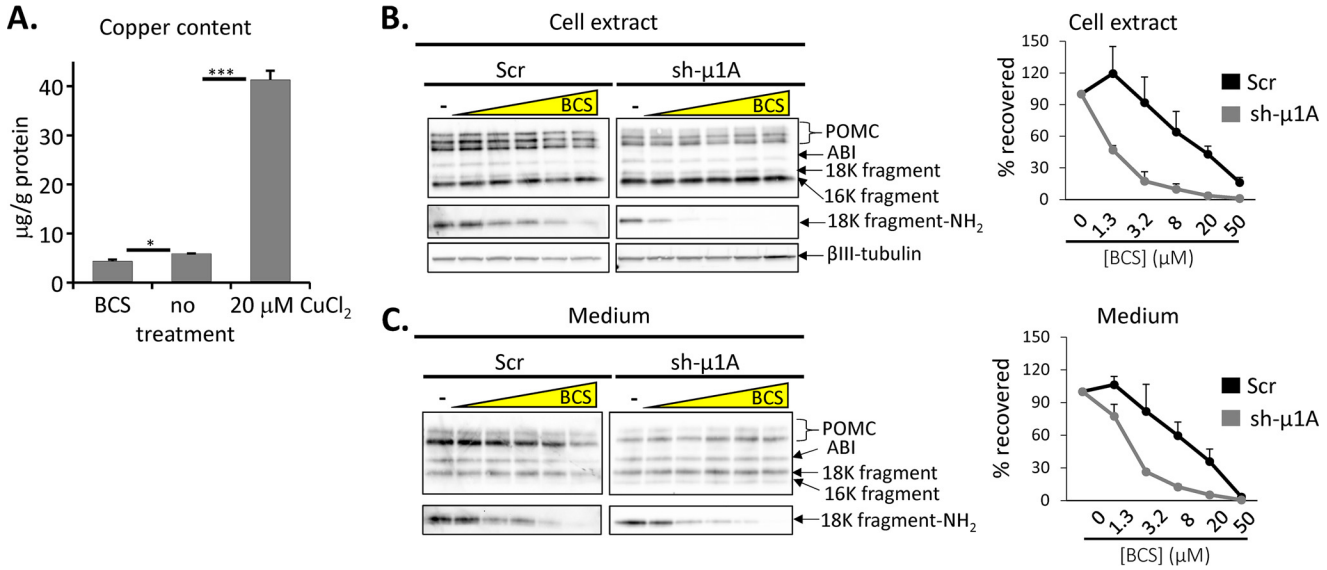

FIGURE 5. **Amidation of 18-kDa fragment is more sensitive to BCS in sh-μ1A PAM-1 cells than in scramble PAM-1 cells.** *A,* copper levels in AtT-20 cells after treatment with 50 μM BCS overnight, 20 μM $CuCl_2$ for 2 h, or untreated as a control ($n = 4$, *, $p < 0.05$; ***, $p < 0.001$). Scramble and sh-μ1A PAM-1 cells were treated with increasing amounts of BCS overnight. Cell extracts (*B*) and media (*C*) were collected and analyzed using the NH_2-specific and γ_3MSH-specific antibodies. βIII-tubulin was used as a loading control. Levels of 18-kDa fragment-NH_2 decreased as the concentration of BCS increased. Duplicate wells from three separate experiments were analyzed; for both cell extracts (*graph* in *B*) and media (*graph* in *C*), levels of 18-kDa fragment-NH_2 were expressed as a percentage of the control sample.

Amidation of 18-kDa fragment secreted into the medium throughout the entire time of exposure to BCS showed a similar increase in the sensitivity of sh-μ1A PAM-1 cells to BCS (Fig. 5*C*). A 2-fold decrease in the level of AP-1 impaired the ability of AtT-20 cells to provide copper to PAM-1 in the presence of a cell-impermeant copper chelator.

Based on the γ_3MSH pattern in cell lysates (Fig. 5*B*) and spent media (Fig. 5*C*) from scramble and sh-μ1A PAM-1 cells, neither the processing of POMC nor the constitutive-like secretion of its cleavage products differed after treatment with BCS. With no apparent differences in cellular copper levels in scramble and sh-μ1A PAM-1 cells and only a modest decline in Atp7a levels, we explored the possibility that altered PAM-1 and Atp7a trafficking, which could minimize their co-localization, contributed to the increased sensitivity of amidation to BCS in sh-μ1A PAM-1 cells.

PAM-1 Endocytic Cleavage and Surface Localization Are Altered in sh-μ1A PAM-1 Cells—PAM-1 deposited on the cell surface during exocytosis is known to traverse the endocytic pathway, returning to the TGN and to the regulated secretory pathway in a process directed by its cytosolic domain. Antisera to the luminal domains of PAM-1 were used in our earlier study to demonstrate increased basal secretion of the soluble PHM domain by sh-μ1A PAM-1 cells; soluble PHM is created when PC1/3 cleaves at a paired basic amino site in the linker region connecting the two catalytic domains (Fig. 6*A*) (7). Antibody to the C terminus of PAM-1 was used to determine whether endocytic pathway cleavages, which generate specific transmembrane/cytosolic domain fragments, also differed in scramble *versus* sh-μ1A PAM-1 cells (Fig. 6*B*). Levels of the transmembrane domain/cytosolic domain fragments generated in secretory granules (Int1) and in the endocytic pathway (Int2) were both decreased in sh-μ1A PAM-1 cells compared with scramble PAM-1 cells, suggesting that endocytic trafficking was altered. Overnight incubation with BCS had no effect on the pattern in either cell line (Fig. 6*B*).

We next explored the possibility that plasma membrane levels of PAM-1 differed. To quantify cell surface levels of PAM-1, surface biotinylation experiments were carried out (31). Membrane trafficking was blocked by chilling the cells on ice. Cell surface proteins were biotinylated at 4 °C using cell-impermeable sulfo-NHS-LC-biotin. PAM-1 proteins in total cell lysates and biotinylated PAM-1 in eluates were compared by Western blot analysis (Fig. 6*C*). A 75% increase in PAM-1 cell surface levels was observed in sh-μ1A PAM-1 cells *versus* scramble PAM-1 cells; the amount of PALm on the cell surface doubled in sh-μ1A PAM-1 cells (Fig. 6*C*).

If the His/Met-rich luminal loop of Atp7a transfers copper directly to PAM-1, as suggested by biochemical studies (3, 4), the two proteins must spend some time in the same subcellular compartment. We used co-immunoprecipitation to search for evidence of an interaction. PAM-1 AtT-20 cells were pretreated with 50 μM BCS overnight or 20 μM $CuCl_2$ for 2 h before co-immunoprecipitation to test whether a change in copper levels had any effect on the interaction. Using affinity-purified antibody to the C terminus of Atp7a, PAM-1 could be co-immunoprecipitated after both treatments (Fig. 6*D*). Purified rabbit antibodies were used as a negative control. A small percentage of the PAM-1 interacted with Atp7a (directly or indirectly), and modifying the copper content of the medium had no effect on the interaction.

Endocytic Pathway Is Altered in sh-μ1A PAM-1 Cells—We used light and electron microscopy to search for differences in PAM-1 endocytic trafficking in scramble and sh-μ1A PAM-1 cells. To get an overview of the endocytic pathway, cells incubated with fluorescently tagged transferrin, a marker for early and recycling endosomes, were stained for EEA1, an early endosomal marker (Fig. 7*A*). EEA1 and internalized transferrin were

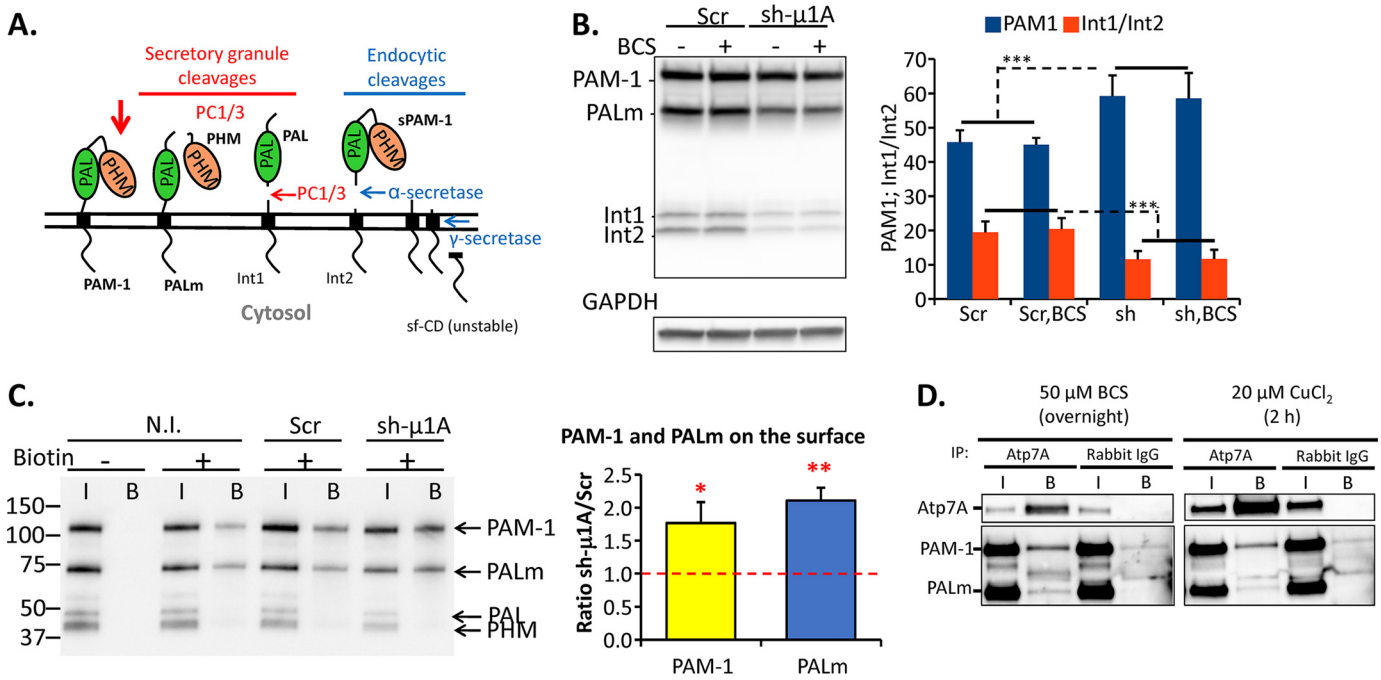

FIGURE 6. **PAM-1 endocytic cleavage and surface localization differ in sh-μ1A PAM-1 cells.** *A,* PAM-1 processing in secretory granules and endosomes. PC1/3 cleavage produces PHM, PALm, PAL, and intermediate 1 (*Int1*). In endosomes, α-secretase cleaves PAM-1, generating soluble PAM-1 (*sPAM-1*) and intermediate 2 (*Int2*). Intermediates 1 and 2 can be cleaved by γ-secretase, producing a soluble fragment of the cytosolic domain (*sf-CD*), which can accumulate in the nucleus (18). *B,* scramble and sh-μ1A PAM-1 cells were incubated in the absence or presence of 50 μM BCS for 16 h before extraction in SDS lysis buffer; Western blot analysis utilized an antibody specific for the C terminus of PAM (*upper panel*) or GAPDH (*lower panel*). Three-way ANOVA compared cell type (Scr, sh-μ1A), treatment (plain, BCS), and molecule (PAM1, Int1/Int2). BCS had no effect on the patterns observed, but sh-μ1A PAM-1 lysates contained increased levels of PAM1 ($n = 4 + 4$; ***, $p < 0.001$) and reduced levels of Int1/Int2 ($n = 4 + 4$; ***, $p < 0.001$). *C,* Western blot of cell surface biotinylation experiment carried out on cells chilled to 4 °C. Streptavidin-bound samples (*B*) represent 125 times more material than input (*I*) samples. The antibody used recognizes the region between PHM and PAL. *N.I.,* noninfected PAM-1 cells. The *graph* shows the ratio of PAM-1 and PALm cell surface levels in sh-μ1A PAM-1 cells over scramble PAM-1 cells. The *dotted line* indicates what PAM-1 and PALm cell surface levels would be if they were identical in scramble and sh-μ1A PAM-1 cells ($n = 3$, **, $p < 0.01$; *, $p < 0.05$). *D,* co-immunoprecipitation of PAM-1 and Atp7a. PAM-1 AtT-20 cells were treated with either 50 μM BCS overnight or 20 μM $CuCl_2$ for 2 h before extraction in TMT. Cell lysates were incubated with Atp7a antibody. Rabbit IgG was used as a control. The amount of input analyzed represents 1/20th of the amount of immunoprecipitate (*IP*) analyzed (*I*, input; *B*, bound).

largely co-localized in both cell lines. In scramble PAM-1 cells, puncta were evenly spread throughout the cell, with only a slight accumulation near the nucleus. In contrast, in sh-μ1A PAM-1 cells, puncta were concentrated near the nucleus.

Endosomes move along microtubules, driven by kinesin or dynein motors; in general, dynein motors bring organelles to the cell center, whereas kinesin motors carry them toward the cell periphery (42). A role for AP-1 in connecting endosomes to specific kinesin motors has been reported (43, 44). To test the hypothesis that the perinuclear localization of early endosomes observed in sh-μ1A PAM-1 cells reflected altered microtubule-dependent transport, cells were treated with nocodazole, a microtubule-destabilizing agent that can be used to eliminate microtubule-dependent trafficking of endosomes (Fig. 7*B*) (34). After nocodazole treatment, internalized transferrin was diffusely distributed in both cell lines. The microtubule-dependent trafficking of early/recycling endosomes was impaired in sh-μ1A PAM-1 cells.

We next explored the endocytic pathway in these two cell lines using electron microscopy. To identify endocytic compartments, scramble and sh-μ1A PAM-1 cells were incubated with WGA tagged with HRP. In both cell lines, early endosomes were highly tubulated, and WGA-HRP reached the TGN during a 10-min incubation at 37 °C (Fig. 7*C*).

PAM-1 Endocytic Trafficking Is Perturbed in sh-μ1A PAM-1 Cells—We next utilized light and electron microscopy to explore the endocytic trafficking of PAM-1 in scramble and sh-μ1A PAM-1 cells in more detail. PAM-1 trafficking through the endosomal pathway was first studied by incubating cells with a PAM ectodomain antibody and fluorescently tagged transferrin (Fig. 8*A*). In both cell lines, the PAM/antibody-positive puncta largely co-localized with transferrin-positive puncta. As observed above, puncta accumulated near the Golgi complex in sh-μ1A cells and were more dispersed in scramble PAM-1 cells.

The Golgi region of AtT-20 cells includes immature secretory granules as well as a complex mixture of endocytic compartments (31, 32). Methods for quantifying the trafficking of PAM·antibody complexes formed on the cell surface through early endosomes and into multivesicular bodies were developed previously, revealing regulated movement of these complexes from the external membrane of the multivesicular body into intraluminal vesicles (31). This approach was used to compare PAM trafficking in scramble and sh-μ1A PAM-1 cells; cells incubated with gold-tagged PAM antibody complexes at 4 °C were then incubated at 37 °C for 10 or 20 min (Fig. 8*B*). Gold particles could be identified in multivesicular bodies and lysosomes (Fig. 8*C*). Progression of PAM·Ab-gold complexes from

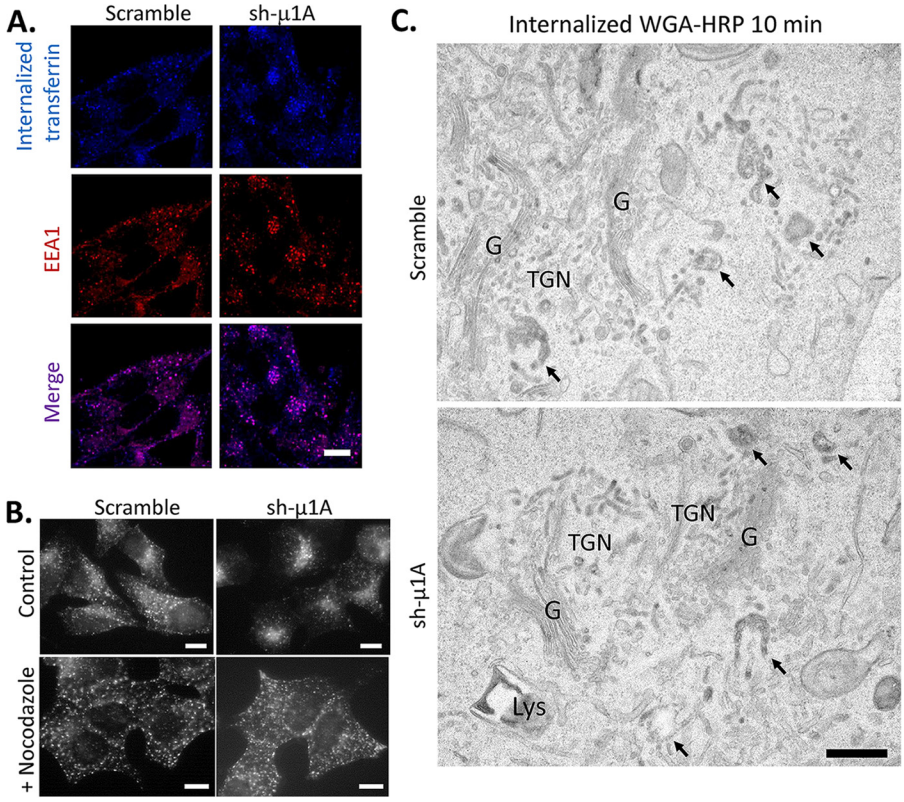

FIGURE 7. **Endocytic pathway is altered in sh-μ1A PAM-1 cells.** *A,* scramble and sh-μ1A PAM-1 cells were incubated with 25 μg/ml Alexa Fluor 546 transferrin for 10 min at 37 °C before fixation and then stained for EEA1. Strong co-localization of EEA1 and transferrin was observed in both cell lines. Internalized transferrin formed a cluster of vesicles near the nucleus in sh-μ1A PAM-1 cells, whereas transferrin-positive vesicles were evenly distributed throughout scramble PAM-1 cells. *Scale bar,* 10 μm. *B,* scramble and sh-μ1A PAM-1 cells were pretreated with 10 μM nocodazole for 20 min or remained in serum-free medium (*control*) before being incubated with Alexa Fluor 546 transferrin as described above. Nocodazole treatment prevented the peri-nuclear accumulation of transferrin-positive puncta observed in sh-μ1A PAM-1 cells. *Scale bar,* 10 μm. *C,* scramble and sh-μ1A PAM-1 cells were incubated with WGA tagged with horseradish peroxidase (*HRP*) for 10 min at 37 °C before fixation and visualization of peroxidase-catalyzed production of oxidized diaminobenzidine by transmission EM. In both cell lines, highly tubulated structures (shown by arrows) were labeled; labeled tubules were also present in the TGN. *Scale bar,* 500 nm.

early endosomes to multivesicular bodies was similar in scramble and sh-μ1A PAM-1 cells. After 20 min of internalization, the percentage of gold particles co-localized with lysosomes was higher in sh-μ1A PAM-1 cells than in scramble PAM-1 cells, although the percentage of gold particles on the external membrane of multivesicular bodies was lower (Fig. 8*D*). PAM trafficking through this part of the endocytic pathway differed in scramble and sh-μ1A PAM-1 cells.

The PAM·Ab-gold complexes cannot be used to detect the movement of PAM from endosomes back to the TGN (31). Because the methods used to visualize this trafficking step at the EM level (detection of internalized PAM antibody using nanogold particles and silver intensification) cannot be used for quantification, we turned to immunofluorescence to evaluate this aspect of the endocytic trafficking of PAM. At steady state, PAM co-localized with syntaxin 6 in the Golgi/TGN area in both scramble and sh-μ1A PAM-1 cells (Fig. 8*E*). The time course over which internalized PAM·Ab complexes co-localized with syntaxin 6 was quantified; no difference was observed between scramble and sh-μ1A PAM-1 cells (Fig. 8*F*). Despite the perinuclear accumulation of early endosomes in sh-μ1A PAM-1 cells, the kinetics of PAM return to a syntaxin 6-positive compartment were similar in both cell lines.

Atp7a Distribution Is Altered in sh-μ1A PAM-1 Cells—In fibroblasts from MEDNIK patients and HeLa cells with reduced μ1A levels, the steady state localization of ATP7A is altered; instead of concentrating in the Golgi region, ATP7A is dispersed throughout the cell. To determine whether Atp7a localization depended on AP-1 function in AtT-20 cells, scramble and sh-μ1A PAM-1 cells were stained for Atp7a. In both cell lines, Atp7a was concentrated in the Golgi area (Fig. 9*A*).

We had expected to see a role for AP-1 in Atp7a trafficking in AtT-20 cells. As described above for PAM-1, Atp7a is retrieved from the plasma membrane by endocytosis. The 20% drop in steady state levels of Atp7a in sh-μ1A PAM-1 cells suggested a change in its turnover. To determine whether Atp7a endocytic trafficking differed in sh-μ1A PAM-1 cells, fluorescently tagged transferrin was again used to label early/recycling endosomes; in order to disperse the endosomes that accumulate in the perinuclear region of sh-μ1A cells, cells were exposed to a low dose of nocodazole before the addition of transferrin (Fig. 9*B*). We then used confocal microscopy to evaluate co-localization of internalized transferrin and Atp7a in scramble and sh-μ1A PAM-1 cells (Fig. 9*B*). Quantification of images revealed an increase in the co-localization of Atp7a and internalized transferrin in sh-μ1A PAM-1 cells (18 $\pm$ 2% *versus* 28 $\pm$ 3% co-localization). In AtT-20 cells, as in HeLa cells, a decrease in AP-1 function resulted in the accumulation of Atp7a in an early/recycling endosomal compartment (11).

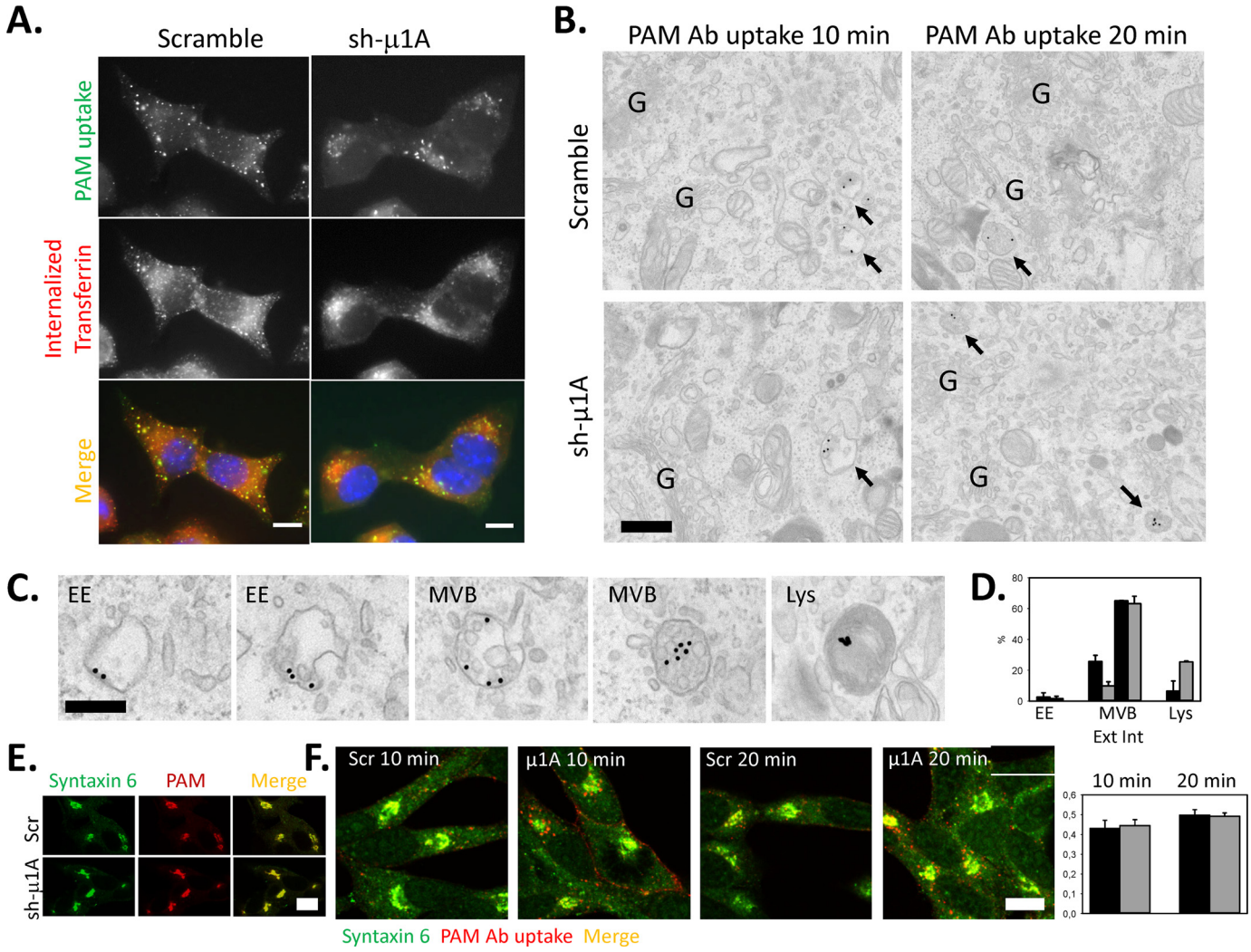

FIGURE 8. **Internalization of PAM-1 is altered in sh-μ1A PAM-1 cells.** *A,* scramble and sh-μ1A PAM-1 cells were incubated with PAL antibody (1:50 dilution) and 25 μg/ml Alexa Fluor 546 transferrin for 10 min at 37 °C. Fixed cells were permeabilized, and secondary antibody (FITC anti-rabbit) was added to examine the distribution of internalized PAL antibody. Strong co-localization of internalized antibody and transferrin was observed in both cell lines. Internalized transferrin formed a cluster of vesicles near the nucleus in sh-μ1A PAM-1 cells, whereas transferrin-positive vesicles were more evenly distributed throughout scramble PAM-1 cells. *Scale bar,* 10 μm. *B,* cell membrane of scramble and sh-μ1A PAM-1 cells was labeled with PAM antibody (1:250 dilution) and 15 nm protein A-gold at 4 °C; PAM Ab·gold complexes were then allowed to traffic normally for 10 or 20 min at 37 °C before fixation. *Arrows* indicate gold-labeled endosomes; *G* = Golgi stack. *Scale bar,* 0.5 μm. *C,* PAM Ab·gold complex containing endosomal structures were classified as early endosomes (*EE*, vacuolar with 0–2 intraluminal vesicles in the plane of the section), multivesicular bodies (*MVB*), and lysosomes (*Lys*); representative images are shown in the panel. *Scale bar,* 0.2 μm. *D,* percent of total gold particles in early endosomes, at the external membrane (*Ext*), or with the intraluminal vesicles (*Int*) of multivesicular bodies and in lysosomes in scramble (*black bars*) and sh-μ1A PAM-1 cells (*gray bars*) (mean ± S.E. from two separate experiments). *E,* steady state localization of syntaxin 6, a TGN marker, corresponds to the steady state localization of PAM in scramble and sh-μ1A PAM-1 cells. *F,* scramble and sh-μ1A PAM-1 cells were allowed to internalize PAM antibody for 10 or 20 min. *Scale bars,* 10 μm. The extent to which internalized PAM antibody staining overlapped steady state syntaxin 6 staining was evaluated using Manders' coefficient; no difference between scramble and sh-μ1A PAM-1 cells was observed after 10 or 20 min of internalization (mean ± S.E. from three separate experiments).

Copper-dependent Atp7a Trafficking Differs in Neuroendocrine Cells and HeLa Cells—When fibroblasts or HeLa cells are treated with elevated levels of copper, Atp7a shifts from the Golgi region to the cell periphery; when these cells are treated with a copper chelator, such as BCS, Atp7a accumulates in the Golgi region (14, 45). AtT-20 cells were treated with 20 μM $CuCl_2$ for 2 h or with 50 μM BCS overnight, and endogenous Atp7a was then localized by immunofluorescent staining (Fig. 10*A*). Even after exposure to high levels of $CuCl_2$, Atp7a was largely localized in the Golgi area in AtT-20 cells; the effects of 20 and 200 μM $CuCl_2$ (data not shown) were similar. Although a major shift of Atp7a toward the plasma membrane was not observed, exposure to elevated levels of copper did affect the localization of Atp7a. The ratio of average fluorescent intensity for Atp7a in the cytosol (any part of the cell excluding the Golgi and nucleus) to average intensity in the Golgi area increased by 2-fold upon treatment with $CuCl_2$; this ratio was not altered by BCS treatment (Fig. 10*A*). Treatment with 200 μM $CuCl_2$ did not have a greater effect on this ratio than treatment with 20 μM $CuCl_2$; most Atp7a was still located in the perinuclear region.

Because Atp7a trafficking differed in AtT-20 cells and HeLa cells, we turned to rat primary anterior pituitary cultures to ask whether this difference in Atp7a trafficking was common to peptide-producing cells. Primary pituitary cells were cultured *in vitro* for 4 days before being treated with 50 μM BCS overnight or 20 μM $CuCl_2$ for 2 h; control cells remained in normal

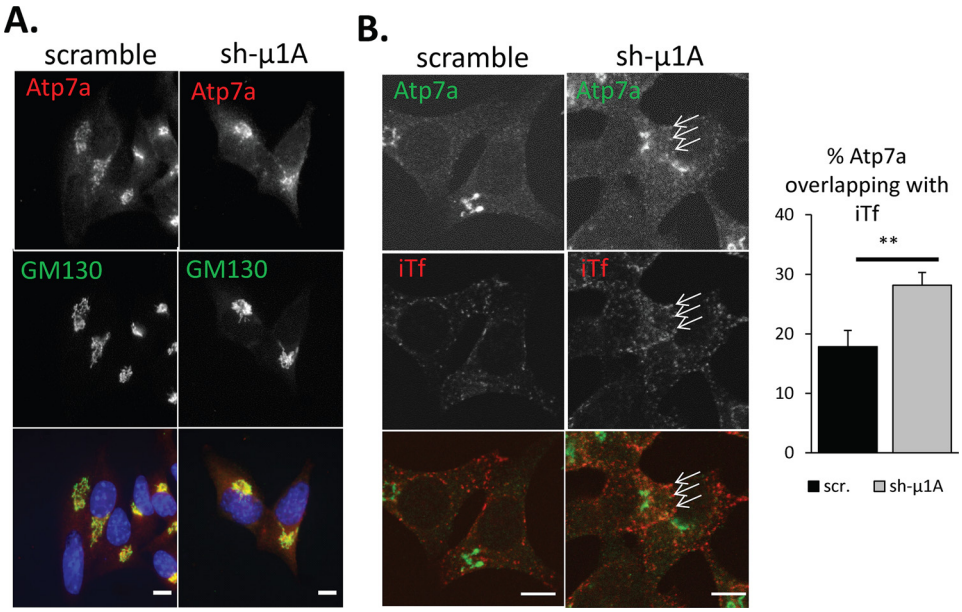

FIGURE 9. **Atp7a endocytic trafficking is altered in sh-μ1A PAM-1 cells.** *A,* steady state localization of Atp7a (Cy3 anti-rabbit) and GM130 (FITC anti-mouse) in scramble and sh-μ1A PAM-1 cells. *B,* confocal images of indirect immunofluorescent staining of Atp7a (FITC anti-rabbit) and internalized Alexa Fluor 546 transferrin (*iTf*) in scramble and sh-μ1A PAM-1 cells after treatment for 20 min with medium containing 0.05% DMSO (control) or 10 μM nocodazole in 0.05% DMSO. Nuclei were stained with Hoechst; *white arrows* indicate co-localization of internalized transferrin and Atp7a. *Scale bar,* 10 μm. *Graph*: % Atp7a area overlapping with internalized transferrin was increased in sh-μ1A *versus* scramble PAM-1 cells; (Student's *t* test, **, $p < 0.01$, $n = 10$).

medium. Treatment of primary pituitary cells with elevated levels of copper did not result in a shift of any significant fraction of the Atp7a to the cell surface (Fig. 10*B*).

We next asked whether Atp7a trafficking responded to elevated copper levels in sh-μ1A PAM-1 cells. Scramble and sh-μ1A PAM-1 cells were treated with 50 μM BCS overnight or with 20 μM $CuCl_2$ for 2 h. Immunofluorescent staining was then used to evaluate the effect of elevated copper on Atp7a localization (Fig. 10*C*). Both scramble and sh-μ1A PAM-1 cells exposed to 20 μM $CuCl_2$ for 2 h showed a similar slight, but reproducible, shift of Atp7a away from the perinuclear region and toward the cell periphery (Fig. 10*C*, *graph*).

To confirm the immunofluorescence data, surface biotinylation and Western blots were used to quantify the levels of Atp7a in the cell and at the cell surface after exposure to 20 μM $CuCl_2$ for 2 h (Fig. 10*D*). SNAP25, an intracellular protein, was used as a negative control to ensure that copper exposure did not damage the cells. The total cell lysate (input) showed a 2–3-fold increase in Atp7a levels following copper exposure (Fig. 10*E*), even though quantitative PCR analysis showed no change in Atp7A mRNA (data not shown). Biotinylated Atp7a was captured on streptavidin beads; when compared with the amount of Atp7a in the corresponding lysate, only 0.1% of the total Atp7a could be identified on the cell surface at steady state. The results of our surface biotinylation experiments are in agreement with our immunofluorescence data. Atp7a cell surface levels increased 3-fold when either scramble or sh-μ1A PAM-1 cells were exposed to 20 μM $CuCl_2$ (Fig. 10*F*). Taken together, the copper-dependent trafficking of Atp7a to the plasma membrane was not altered in sh-μ1A PAM-1 cells.

Discussion

PAM-1 Function Is More Sensitive to Copper Restriction When AP-1 Levels Are Reduced: 18-kDa Fragment-NH_2—Peptide amidation is an essential post-translational modification; neither flies nor mice lacking PAM can complete development (16, 46). Copper is absolutely essential for PAM function. It is clear from studies in mottled brindled mice (47) and yeast (2) that Atp7a delivers copper to PAM, but how and where this process occurs is not known. Although SOD1, a cytosolic cuproenzyme, binds copper with high affinity (~6 fM), the affinity of PHM for copper is 7 orders of magnitude lower (Cu_H ~60 nM); consistent with this, copper bound to PAM is generally lost in cell lysates and during purification (48, 49).

Peptide amidation cannot occur until a peptidylglycine substrate is available. Cleavage of POMC starts in the cisternae of the TGN, where the C terminus of ACTH and the amidated C terminus shared by the 18-kDa fragment and JP can first be visualized (22). Pulse-chase metabolic labeling studies identify immature secretory granules as the major POMC-processing site (50). Short lived biosynthetic intermediates like ABI and 18-kDa fragment can be secreted (constitutive-like secretion) or converted into ACTH and 16-kDa fragment, which are stored in mature secretory granules and released in response to secretagogue. In sh-μ1A PAM-1 cells, immature secretory granules are replaced by noncondensing secretory granules, a cleavage-competent compartment that fails to respond to secretagogues (7). Our ability to assess the amidation of 18-kDa fragment provided a window into this copper-dependent step in POMC processing.

Although the extent of amidation of 18-kDa fragment did not differ in Scr *versus* sh-μ1A PAM-1 cells, its sensitivity to inhibition by BCS was substantially greater in sh-μ1A PAM-1 cells.

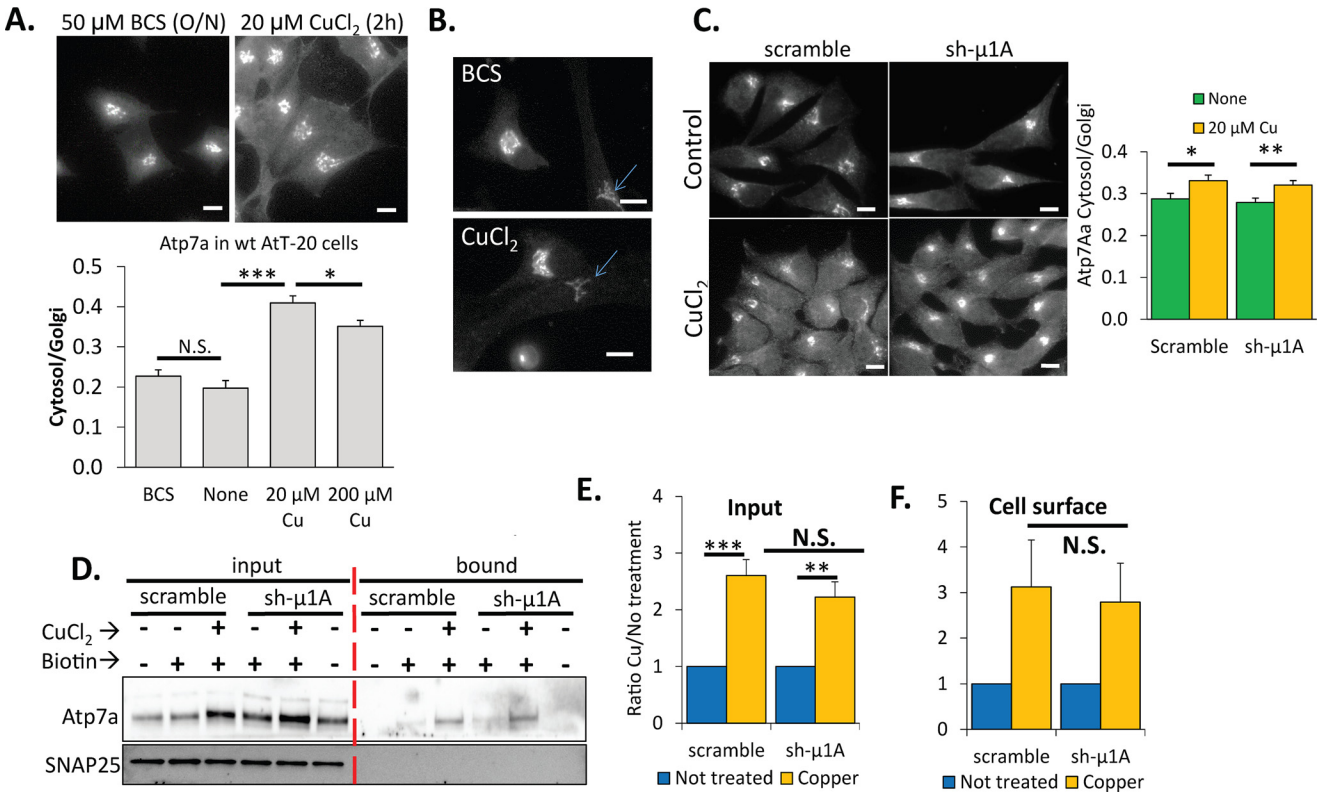

FIGURE 10. **Copper-dependent trafficking of Atp7a in sh-μ1A PAM-1 cells.** *A,* wild type AtT-20 cells treated with 50 μM BCS overnight or with 20 μM $CuCl_2$ for 2 h were fixed and stained for Atp7a (Cy3 anti-rabbit). *Graph* shows the ratio for mean Atp7a fluorescence intensity in the cytosol (any part of the cell, excluding nucleus and Golgi) and the Golgi region. A 50% increase in the ratio was observed when cells were treated with copper. Treatment with BCS did not alter the ratio ($n = 8–25$; ***, $p < 0.001$; *, $p < 0.05$). Cells were visualized using a Nikon TE300 epifluorescence microscope. *B,* rat primary pituitary cells treated with 50 μM BCS overnight (*top*) or with 20 μM $CuCl_2$ (*bottom*) for 2 h were fixed and stained for Atp7a (Cy3 anti-rabbit) and GM130 (*cis*-Golgi, FITC anti-mouse). Atp7a distribution was not detectably altered by BCS or copper treatment (*blue arrows* point to fibroblasts; *scale bar,* 10 μm). *C,* scramble and sh-μ1A PAM-1 cells treated with 20 μM $CuCl_2$ for 2 h or untreated were fixed and stained for Atp7a (C terminus, Cy3 anti-rabbit). Cells were visualized using a Nikon TE300 epifluorescence microscope. *Graph* shows the ratio for mean Atp7a fluorescence intensity in the cytosol over the Golgi region. An increase in the ratio was observed when either cell type was treated with copper ($n = 35–44$; *, $p < 0.05$; **, $p < 0.01$). *D,* cell surface biotinylation after treatment of scramble and sh-μ1A PAM-1 cells with 20 μM $CuCl_2$ for 2 h. Streptavidin-bound samples represent 100 times more material than *input* samples; Atp7a was visualized on the *upper part* of the blot and SNAP25, an intracellular protein used as a negative control, on the *bottom part*. *E,* increase in total Atp7a signal in response to elevated copper was observed in both scramble and sh-μ1A PAM-1 cells; $n = 4$; ***, $p < 0.001$; **, $p < 0.01$. *F,* cell surface levels of Atp7a as a % of input levels rose in a similar manner in response to exposure to $CuCl_2$ in both scramble and sh-μ1A PAM-1 cells; $n = 3–4$. *N.S.,* not significant.

The total copper content of Scr and sh-μ1A PAM-1 cells did not differ, eliminating it as causative factor. This observation is consistent with the fact that the copper content of fibroblasts was unaffected by loss of the σ1A subunit of AP-1 (1). Overnight incubation of AtT-20 cells with 50 μM BCS only reduced copper content to about 70% of control, but totally eliminated PAM-1 function in Scr and sh-μ1A cells, indicating that luminal copper homeostasis was very sensitive to BCS. It is not clear whether the mobile pool of copper, which is known to play an important role in signaling (51), and luminal copper are similarly affected by incubation with BCS.

Constitutive-like Secretion of POMC Products Is Altered When AP-1 Levels Are Reduced—The POMC products stored in Scr and sh-μ1A PAM-1 cells did not differ. Although the basal rate of secretion of all of the POMC products recognized by the γ_3MSH-specific antibody did not differ, the products released by sh-μ1A PAM-1 cells were more extensively cleaved. Despite this, the extent to which 18-kDa fragment was amidated did not differ.

Constitutive-like secretion of ABI and 18-kDa fragment must occur from a cleavage-competent compartment. The exit of newly synthesized POMC from the TGN and its access to a cleavage-competent compartment can be blocked by incubation at 20 °C (50). Immature secretory granules in Scr PAM-1 cells and noncondensing secretory granules in sh-μ1A PAM-1 cells are expected to be the major source of constitutive-like secretion of ABI and 18-kDa fragment. Although PAM accumulates in the noncondensing secretory granules found near the surface of sh-μ1A PAM-1 cells, Atp7a does not. Consistent with this observation, Atp7a does not accumulate in mature secretory granules in AtT-20 cells or primary corticotropes. Very little of the 18-kDa fragment is stored in AtT-20 cells; PAM must be metallated and available to amidate 18-kDa fragment-Gly as it exits the cleavage competent compartment where it was created.

Diminished AP-1 Levels Alter PAM Endocytic Trafficking in Neuroendocrine Cells—If Atp7a delivers copper directly to PAM, as proposed (4), transfer could occur in the TGN or in an endocytic compartment. The proper endocytic trafficking of both proteins requires AP-1. Although transferrin internalized by Scr PAM-1 cells appeared in puncta distributed throughout the cell, transferrin internalized by sh-μ1A PAM-1 cells was largely localized to the perinuclear region. We observed an

increase in the presence of Atp7a in these endosomes, but no accumulation of PAM-1.

AP-1 accumulates at the tubular domains of early endosomes, and knockdown of Arf1, which mediates its binding, causes the formation of elongated tubules (52). We did not see an effect on tubulation from early endosomes when AP-1 levels were decreased. Endosomes move along microtubules, with dynein bringing cargo to their minus ends (from the cell periphery to the cell center), and most kinesins bringing cargo to the plus end of microtubules (from the cell center to the cell periphery). Endosomes are connected to microtubules by multiple cytosolic proteins, including AP-1, which interacts with microtubule-associated protein 1a and the kinesin 3 member, KIF13A (43, 44). Lack of AP-1 to connect kinesins with endosomes could contribute to the accumulation of endosomes in the cell center. The interaction of AP-3 with actin-bound Septin6 and Septin7 acts as a brake, preventing premature translocation of early endosomes (53). The increased constitutive-like secretion of POMC products and enhanced trafficking of PAM through late endosomes suggest that AP-1 may also serve as a brake.

The endocytic trafficking of plasma membrane PAM-1 is affected both by its luminal and cytosolic domains (31, 54). Following clathrin-mediated endocytosis, internalized PAM-1 appears on the limiting membrane of multivesicular bodies and then in intraluminal vesicles, the TGN, and secretory granules (31). If PAM-1 retrieved from the plasma membrane loses one or both of its copper ions, copper could again be provided as the protein traverses the endocytic pathway. In this study, we observed an increase in PAM-1 cell surface levels in sh-μ1A PAM-1 cells. Because PAM-1 does not bind copper tightly, its increased exposure to BCS and loss of copper while on the cell surface could contribute to the reduced ability of these cells to produce amidated product when exposed to BCS.

Diminished AP-1 Levels Alter Atp7a Endocytic Trafficking in Neuroendocrine Cells—In HeLa cells, internalized transferrin concentrated in the perinuclear Golgi region when expression of one AP-1 subunit was decreased (56). A similar response was observed in fibroblasts isolated from μ1A knock-out mice, where early endosomes tend to collect near the nucleus (11). By using nocodazole to disrupt microtubule-dependent endosomal trafficking (57), we observed an increase in the co-localization of Atp7a and internalized transferrin in sh-μ1A PAM-1 cells compared with scramble PAM-1 cells. As in other cell types, the retrieval of Atp7a from the endocytic pathway in AtT-20 cells appears to require AP-1. PAM does not accumulate in the same organelle, limiting its access to Atp7a. The decreased retrieval of Atp7a from endocytic compartments may result in its increased degradation, accounting for its reduced steady state level in sh-μ1A PAM-1 cells. We also observed a decrease in the steady state level of APP in sh-μ1A PAM-1 cells. APP trafficking is controlled by SorLA, a member of the Vps10-domain receptor family, whose trafficking between the Golgi and endosome is also AP-1-dependent (58, 59). As for Atp7a, AP-1 may indirectly help protect APP from degradation. The cation-independent mannose 6-phosphate receptor (MPR300), which cycles between the plasma membrane and the TGN, was affected differently by μ1A depletion; its internalization rate increased and it accumulated in early endosomes (55).

The effect of copper on Atp7a trafficking is cell type-specific. In HeLa cells and fibroblasts exposed to elevated levels of copper, a significant fraction of the ATP7A moved to the cell surface (6, 45). Under normal conditions, levels of Atp7a on the surface of AtT-20 cells are very low, and no increase was observed in sh-μ1A PAM-1 cells. A small fraction of the Atp7a in AtT-20 cells and primary pituitary cells moved to the cell periphery in response to elevated copper levels, but the vast majority remained in vesicular structures localized to the Golgi region. Atp7a in Scr and sh-μ1A PAM-1 cells responded in a similar manner to elevated copper. This difference may reflect the need to ensure that secretory granule cuproenzymes like PAM-1 acquire copper effectively. In MNT-1 human melanoma cells, ATP7A localizes to melanosomes, where tyrosinase, a cuproenzyme required for melanin synthesis, resides (29). In the absence of BLOC-1 (biogenesis of lysosome-related organelle complex 1), ATP7A accumulates in early endosomes instead of melanosomes, indicating that AP-1 is not the sole player governing its endocytic trafficking (29).

Our knowledge of the processing steps required to create 18-kDa fragment-Gly from POMC and our understanding of the role of AP-1 in the complex trafficking itineraries of PAM-1 and Atp7a support the hypothesis that copper transported from the cytosol into the lumen of the secretory pathway, which lacks known copper chaperones, can be delivered directly to PAM. Co-immunoprecipitation of a small fraction of the PAM-1 and Atp7a lends support to this model. Impairing AP-1 function in a neuroendocrine cell line revealed significant changes in the steady state levels and trafficking of three cuproproteins, PAM, Atp7a, and APP. The sensitivity of peptide amidation to copper availability could limit peptidergic signaling, contributing to the complex phenotype observed when AP-1 function is compromised.

Author Contributions—M. L. B. designed the study, carried out and analyzed most of the cell culture, biochemical, and immunofluorescence studies, and wrote the paper. N. B. carried out and analyzed all of the experiments involving electron microscopy and wrote the paper. M. E. D. and M. R. carried out all of the metal analyses reported. R. E. M. and B. A. E. conceived of and designed the study, developed the amide-specific assay, and wrote the paper. All authors reviewed the results and approved the final version of the manuscript.

Acknowledgments—We thank Darlene D'Amato for incomparable technical assistance and the Electron Microscopy Unit of the Institute of Biotechnology, University of Helsinki, for providing laboratory facilities.

References

1. Martinelli, D., and Dionisi-Vici, C. (2014) AP1S1 defect causing MEDNIK syndrome: a new adaptinopathy associated with defective copper metabolism. *Ann. N.Y. Acad. Sci.* **1314,** 55–63
2. El Meskini, R., Culotta, V. C., Mains, R. E., and Eipper, B. A. (2003) Supplying copper to the cuproenzyme peptidylglycine α-amidating monooxygenase. *J. Biol. Chem.* **278,** 12278–12284
3. Barry, A. N., Otoikhian, A., Bhatt, S., Shinde, U., Tsivkovskii, R., Black-

burn, N. J., and Lutsenko, S. (2011) The lumenal loop Met-672–Pro-707 of copper-transporting ATPase ATP7A binds metals and facilitates copper release from the intramembrane sites. *J. Biol. Chem.* **286,** 26585–26594
4. Otoikhian, A., Barry, A. N., Mayfield, M., Nilges, M., Huang, Y., Lutsenko, S., and Blackburn, N. J. (2012) Lumenal loop M672-P707 of the Menkes protein (ATP7A) transfers copper to peptidylglycine monooxygenase. *J. Am. Chem. Soc.* **134,** 10458–10468
5. Bousquet-Moore, D., Ma, X. M., Nillni, E. A., Czyzyk, T. A., Pintar, J. E., Eipper, B. A., and Mains, R. E. (2009) Reversal of physiological deficits caused by diminished levels of peptidylglycine α-amidating monooxygenase by dietary copper. *Endocrinology* **150,** 1739–1747
6. Holloway, Z. G., Velayos-Baeza, A., Howell, G. J., Levecque, C., Ponnambalam, S., Sztul, E., and Monaco, A. P. (2013) Trafficking of the Menkes copper transporter ATP7A is regulated by clathrin-, AP-2-, AP-1-, and Rab22-dependent steps. *Mol. Biol. Cell* **24,** 1735–1748
7. Bonnemaison, M., Bäck, N., Lin, Y., Bonifacino, J. S., Mains, R., and Eipper, B. (2014) AP-1A controls secretory granule biogenesis and trafficking of membrane secretory granule proteins. *Traffic* **15,** 1099–1121
8. Canuel, M., Lefrancois, S., Zeng, J., and Morales, C. R. (2008) AP-1 and retromer play opposite roles in the trafficking of sortilin between the Golgi apparatus and the lysosomes. *Biochem. Biophys. Res. Commun.* **366,** 724–730
9. Robinson, M. S., Sahlender, D. A., and Foster, S. D. (2010) Rapid inactivation of proteins by rapamycin-induced rerouting to mitochondria. *Dev. Cell* **18,** 324–331
10. Zizioli, D., Meyer, C., Guhde, G., Saftig, P., von Figura K., and Schu, P. (1999) Early embryonic death of mice deficient in γ-adaptin. *J. Biol. Chem.* **274,** 5385–5390
11. Meyer, C., Zizioli, D., Lausmann, S., Eskelinen, E. L., Hamann, J., Saftig, P., von Figura K., and Schu, P. (2000) mu1A-adaptin-deficient mice: lethality, loss of AP-1 binding, and rerouting of mannose 6-phosphate receptors. *EMBO J.* **19,** 2193–2203
12. Heldwein, E. E., Macia, E., Wang, J., Yin, H. L., Kirchhausen, T., and Harrison, S. C. (2004) Crystal structure of the clathrin adaptor protein 1 core. *Proc. Natl. Acad. Sci. U.S.A.* **101,** 14108–14113
13. Montpetit, A., Côté, S., Brustein, E., Drouin, C. A., Lapointe, L., Boudreau, M., Meloche, C., Drouin, R., Hudson, T. J., Drapeau, P., and Cossette, P. (2008) Disruption of AP1S1, causing a novel neurocutaneous syndrome, perturbs development of the skin and spinal cord. *PLoS Genet.* **4,** e1000296
14. Martinelli, D., Travaglini, L., Drouin, C. A., Ceballos-Picot, I., Rizza, T., Bertini, E., Carrozzo, R., Petrini, S., de Lonlay, P., El Hachem, M., Hubert, L., Montpetit, A., Torre, G., and Dionisi-Vici, C. (2013) MEDNIK syndrome: a novel defect of copper metabolism treatable by zinc acetate therapy. *Brain* **136,** 872–881
15. Hellman, N. E., and Gitlin, J. D. (2002) Ceruloplasmin metabolism and function. *Annu. Rev. Nutr.* **22,** 439–458
16. Czyzyk, T. A., Ning, Y., Hsu, M. S., Peng, B., Mains, R. E., Eipper, B. A., and Pintar, J. E. (2005) Deletion of peptide amidation enzymatic activity leads to edema and embryonic lethality in the mouse. *Dev. Biol.* **287,** 301–313
17. Steveson, T. C., Ciccotosto, G. D., Ma, X. M., Mueller, G. P., Mains, R. E., and Eipper, B. A. (2003) Menkes protein contributes to the function of peptidylglycine α-amidating monooxygenase. *Endocrinology* **144,** 188–200
18. Francone, V. P., Ifrim, M. F., Rajagopal, C., Leddy, C. J., Wang, Y., Carson, J. H., Mains, R. E., and Eipper, B. A. (2010) Signaling from the secretory granule to the nucleus: Uhmk1 and PAM. *Mol. Endocrinol.* **24,** 1543–1558
19. Maltese, J. Y., and Eipper, B. A. (1992) Developmental expression of peptidylglycine α-amidating monooxygenase (PAM) in primary cultures of neonatal rat cardiocytes: a model for studying regulation of PAM expression in the rat heart. *Mol. Endocrinol.* **6,** 1998–2008
20. Yun, H. Y., Johnson, R. C., Mains, R. E., and Eipper, B. A. (1993) Topological switching of the COOH-terminal domain of peptidylglycine α-amidating monooxygenase by alternative RNA splicing. *Arch. Biochem. Biophys.* **301,** 77–84
21. Cullen, E. I., and Mains, R. E. (1987) Biosynthesis of amidated joining peptide from pro-adrenocorticotropin-endorphin. *Mol. Endocrinol.* **1,** 583–594
22. Schnabel, E., Mains, R. E., and Farquhar, M. G. (1989) Proteolytic processing of pro-ACTH/endorphin begins in the Golgi complex of pituitary corticotropes and AtT-20 cells. *Mol. Endocrinol.* **3,** 1223–1235
23. Eipper, B. A., Park, L., Keutmann, H. T., and Mains, R. E. (1986) Amidation of joining peptide, a major pro-ACTH/endorphin-derived product peptide. *J. Biol. Chem.* **261,** 8686–8694
24. Milgram, S. L., Kho, S. T., Martin, G. V., Mains, R. E., and Eipper, B. A. (1997) Localization of integral membrane peptidylglycine α-amidating monooxygenase in neuroendocrine cells. *J. Cell Sci.* **110,** 695–706
25. Niciu, M. J., Ma, X. M., El Meskini, R., Ronnett, G. V., Mains, R. E., and Eipper, B. A. (2006) Developmental changes in the expression of ATP7A during a critical period in postnatal neurodevelopment. *Neuroscience* **139,** 947–964
26. Milgram, S. L., Johnson, R. C., and Mains, R. E. (1992) Expression of individual forms of peptidylglycine α-amidating monooxygenase in AtT-20 cells: endoproteolytic processing and routing to secretory granules. *J. Cell Biol.* **117,** 717–728
27. Bolte, S., and Cordelières, F. P. (2006) A guided tour into subcellular colocalization analysis in light microscopy. *J. Microsc.* **224,** 213–232
28. May, V., and Eipper, B. A. (1986) Long term culture of primary rat pituitary adrenocorticotropin/endorphin-producing cells in serum-free medium. *Endocrinology* **118,** 1284–1295
29. Setty, S. R., Tenza, D., Sviderskaya, E. V., Bennett, D. C., Raposo, G., and Marks, M. S. (2008) Cell-specific ATP7A transport sustains copper-dependent tyrosinase activity in melanosomes *Nature* **454,** 1142–1146
30. Mains, R. E., and Eipper, B. A. (1978) Coordinate synthesis of corticotropins and endorphins by mouse pituitary tumor cells. *J. Biol. Chem.* **253,** 651–655
31. Bäck, N., Rajagopal, C., Mains, R. E., and Eipper, B. A. (2010) Secretory granule membrane protein recycles through multivesicular bodies. *Traffic* **11,** 972–986
32. Rajagopal, C., Stone, K. L., Mains, R. E., and Eipper, B. A. (2010) Secretion stimulates intramembrane proteolysis of a secretory granule membrane enzyme. *J. Biol. Chem.* **285,** 34632–34642
33. Luck, A. N., and Mason, A. B. (2012) Transferrin-mediated cellular iron delivery. *Curr. Top. Membr.* **69,** 3–35
34. El Meskini R., Mains, R. E., and Eipper, B. A. (2000) Cell type-specific metabolism of peptidylglycine α-amidating monooxygenase in anterior pituitary. *Endocrinology* **141,** 3020–3034
35. Gaier, E. D., Eipper, B. A., and Mains, R. E. (2013) Copper signaling in the mammalian nervous system: synaptic effects. *J. Neurosci. Res.* **91,** 2–19
36. Acevedo, K. M., Opazo, C. M., Norrish, D., Challis, L. M., Li, Q. X., White, A. R., Bush, A. I., and Camakaris, J. (2014) Phosphorylation of amyloid precursor protein at threonine 668 is essential for its copper-responsive trafficking in SH-SY5Y neuroblastoma cells. *J. Biol. Chem.* **289,** 11007–11019
37. Tanaka, S., Yora, T., Nakayama, K., Inoue, K., and Kurosumi, K. (1997) Proteolytic processing of pro-opiomelanocortin occurs in acidifying secretory granules of AtT-20 cells. *J. Histochem. Cytochem.* **45,** 425–436
38. De, M., Ciccotosto, G. D., Mains, R. E., and Eipper, B. A. (2007) Trafficking of a secretory granule membrane protein is sensitive to copper. *J. Biol. Chem.* **282,** 23362–23371
39. Hamza, I., Prohaska, J., and Gitlin, J. D. (2003) Essential role for Atox1 in the copper-mediated intracellular trafficking of the Menkes ATPase. *Proc. Natl. Acad. Sci. U.S.A.* **100,** 1215–1220
40. Nose, Y., Wood, L. K., Kim, B. E., Prohaska, J. R., Fry, R. S., Spears, J. W., and Thiele, D. J. (2010) Ctr1 is an apical copper transporter in mammalian intestinal epithelial cells *in vivo* that is controlled at the level of protein stability. *J. Biol. Chem.* **285,** 32385–32392
41. Milgram, S. L., Eipper, B. A., and Mains, R. E. (1994) Differential trafficking of soluble and integral membrane secretory granule-associated proteins. *J. Cell Biol.* **124,** 33–41
42. Hirokawa, N., Noda, Y., Tanaka, Y., and Niwa, S. (2009) Kinesin superfamily motor proteins and intracellular transport. *Nat. Rev. Mol. Cell Biol.* **10,** 682–696
43. Nakagawa, T., Setou, M., Seog, D., Ogasawara, K., Dohmae, N., Takio, K., and Hirokawa, N. (2000) A novel motor, KIF13A, transports mannose-6-phosphate receptor to plasma membrane through direct interaction with

AP-1 complex. *Cell* **103,** 569–581
44. Orzech, E., Livshits, L., Leyt, J., Okhrimenko, H., Reich, V., Cohen, S., Weiss, A., Melamed-Book, N., Lebendiker, M., Altschuler, Y., and Aroeti, B. (2001) Interactions between adaptor protein-1 of the clathrin coat and microtubules via type 1a microtubule-associated proteins. *J. Biol. Chem.* **276,** 31340–31348
45. Cobbold, C., Ponnambalam, S., Francis, M. J., and Monaco, A. P. (2002) Novel membrane traffic steps regulate the exocytosis of the Menkes disease ATPase. *Hum. Mol. Genet.* **11,** 2855–2866
46. Jiang, N., Kolhekar, A. S., Jacobs, P. S., Mains, R. E., Eipper, B. A., and Taghert, P. H. (2000) PHM is required for normal developmental transitions and for biosynthesis of secretory peptides in *Drosophila*. *Dev. Biol.* **226,** 118–136
47. Niciu, M. J., Ma, X. M., El Meskini, R., Pachter, J. S., Mains, R. E., and Eipper, B. A. (2007) Altered ATP7A expression and other compensatory responses in a murine model of Menkes disease. *Neurobiol. Dis.* **27,** 278–291
48. Bell, J., El Meskini, R., D'Amato, D., Mains, R. E., and Eipper, B. A. (2003) Mechanistic investigation of peptidylglycine α-hydroxylating monooxygenase via intrinsic tryptophan fluorescence and mutagenesis. *Biochemistry* **42,** 7133–7142
49. Rae, T. D., Schmidt, P. J., Pufahl, R. A., Culotta, V. C., and O'Halloran, T. V. (1999) Undetectable intracellular free copper: the requirement of a copper chaperone for superoxide dismutase. *Science* **284,** 805–808
50. Milgram, S. L., and Mains, R. E. (1994) Differential effects of temperature blockade on the proteolytic processing of three secretory granule-associated proteins. *J. Cell Sci.* **107,** 737–745
51. Dodani, S. C., Domaille, D. W., Nam, C. I., Miller, E. W., Finney, L. A., Vogt, S., and Chang, C. J. (2011) Calcium-dependent copper redistributions in neuronal cells revealed by a fluorescent copper sensor and x-ray fluorescence microscopy. *Proc. Natl. Acad. Sci. U.S.A.* **108,** 5980–5985
52. D'Souza, R. S., Semus, R., Billings, E. A., Meyer, C. B., Conger, K., and Casanova, J. E. (2014) Rab4 orchestrates a small GTPase cascade for recruitment of adaptor proteins to early endosomes. *Curr. Biol.* **24,** 1187–1198
53. Traikov, S., Stange, C., Wassmer, T., Paul-Gilloteaux, P., Salamero, J., Raposo, G., and Hoflack, B. (2014) Septin6 and Septin7 GTP binding proteins regulate AP-3- and ESCRT-dependent multivesicular body biogenesis. *PLoS ONE* **9,** e109372
54. Milgram, S. L., Mains, R. E., and Eipper, B. A. (1996) Identification of routing determinants in the cytosolic domain of a secretory granule-associated integral membrane protein. *J. Biol. Chem.* **271,** 17526–17535
55. Meyer, C., Eskelinen, E. L., Guruprasad, M. R., von Figura, K., and Schu, P. (2001) Mu 1A deficiency induces a profound increase in MPR300/IGF-II receptor internalization rate. *J. Cell Sci.* **114,** 4469–4476
56. Perrin, L., Lacas-Gervais, S., Gilleron, J., Ceppo, F., Prodon, F., Benmerah, A., Tanti, J.-F., and Comont, M. (2013) Rab4b controls an early endosome sorting event by interacting with the γ-subunit of the clathrin adaptor complex 1. *J. Cell Sci.* **126,** 4950–4962
57. Huotari, J., and Helenius, A. (2011) Endosome maturation. *EMBO J.* **30,** 3481–3500
58. Willnow, T. E., and Andersen, O. M. (2013) Sorting receptor SORLA–a trafficking path to avoid Alzheimer disease. *J. Cell Sci.* **126,** 2751–2760
59. Nielsen, M. S., Gustafsen, C., Madsen, P., Nyengaard, J. R., Hermey, G., Bakke, O., Mari, M., Schu, P., Pohlmann, R., Dennes, A., and Petersen, C. M. (2007) Sorting by the cytoplasmic domain of the amyloid precursor protein binding receptor SorLA. *Mol. Biol. Cell* **27,** 6842–6851